NAVAL POSTGRADUATE SCHOOL
Monterey, California

AD-A275 017

THESIS

ACQUISITION TIME ANALYSIS OF NONCOHERENT
PN SEQUENCE ACQUISITION SCHEMES

by

Levent Misirlioglu

September, 1993

Thesis Advisor :   Professor Alex W. Lam

94-02121

94 1 25 018

REPORT DOCUMENTATION PAGE

1a Report Security Classification: Unclassified		1b Restrictive Markings			
2a Security Classification Authority		3 Distribution/Availability of Report			
2b Declassification/Downgrading Schedule		Approved for public release; distribution is unlimited.			
4 Performing Organization Report Number(s)		5 Monitoring Organization Report Number(s)			
6a Name of Performing Organization Naval Postgraduate School	6b Office Symbol 32	7a Name of Monitoring Organization Naval Postgraduate School			
6c Address Monterey, CA 93943-5000		7b Address Monterey, CA 93943-5000			
8a Name of Funding/Sponsoring Organization	6b Office Symbol	9 Procurement Instrument Identification Number			
Address		10 Source of Funding Numbers			
		Program Element No	Project No	Task No	Work Unit Accession No
11 Title ACQUISITION TIME ANALYSIS OF NON-COHERENT PN SEQUENCE ACQUISITION SCHEMES.					
12 Personal Author(s) Levent Misirlioglu					
13a Type of Report Engineer's Thesis	13b Time Covered From To	14 Date of Report 1993 September 23		15 Page Count 90	
16 Supplementary Notation The views expressed in this thesis are those of the author and do not reflect the official policy or position of the Department of Defense or the U.S. Government.					
17 Cosati Codes		18 Subject Terms (continue on reverse if necessary and identify by block number)			
Field	Group	Subgroup	serial search acquisition, spread-spectrum, communications		

19 Abstract

    In direct-sequence spread-spectrum systems, successful communications require phase synchronization of the incoming pseudonoise (PN) coded waveform with a locally generated replica at the receiver. It has been previously shown that sequential PN code acquisition schemes have the potential to achieve the best performance, but they are the least analyzed because of the analytical difficulties.

    The acquisition time for a PN code acquisition scheme is an important parameter for system design purposes. This thesis investigates the performance of two acquisition schemes in terms of the acquisition time. A fixed sample size (FSS) test and a truncated sequential probability ratio test (TSPRT) are studied with noncoherent demodulation in a classical additive white Gaussian noise (AWGN) channel and in presence of fading. Optimal selection of desired detection and false alarm probabilities, the effects of penalty time, majority logic verification schemes and channel signal to noise ratio (SNR) mismatch problems are thoroughly studied using the flow graph technique. Our results show that the TSPRT is efficient, robust (against fading), fast and suitable for real time low cost implementations.

20 Distribution/Availability of Abstract _X_ unclassified/unlimited __ same as report __ DTIC users		21 Abstract Security Classification Unclassified	
22a Name of Responsible Individuals Professor Alex W. Lam		22b Telephone (include Area Code) 408-656-3044	22c Office Symbol EC/LA

DD FORM 1473, 84 MAR   83 APR edition may be used until exhausted   security classification of this page

All other editions are obsolete   Unclassified

Acquisition Time Analysis of
Noncoherent PN Sequence Acquisition Schemes

by

Levent Misirlioglu
Lieutenant Junior Grade, Turkish Navy
B.S., Turkish Naval Academy, 1987

Submitted in partial fulfillment of the
requirements for the degrees of

ELECTRICAL ENGINEER
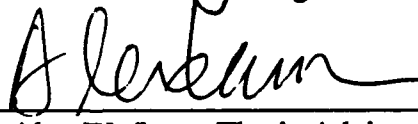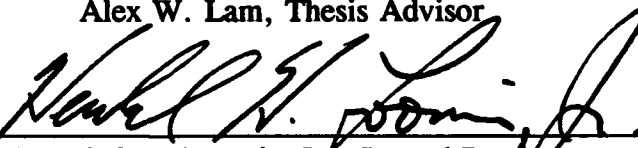and
MASTER OF SCIENCE IN ELECTRICAL ENGINEERING

from the
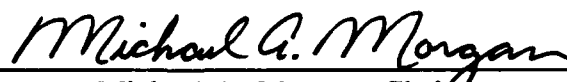
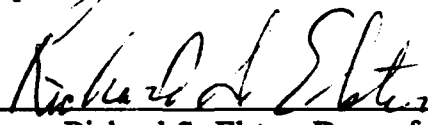NAVAL POSTGRADUATE SCHOOL
September 1993

Author: _____
Levent Misirlioglu

Approved by: _____
Alex W. Lam, Thesis Advisor

_____
Herschel H. Loomis, Jr., Second Reader

_____
Michael A. Morgan, Chairman,
Department of Electrical and Computer Engineering

_____
Richard S. Elster, Dean of Instruction

ABSTRACT

In direct-sequence spread-spectrum systems, successful communications require phase synchronization of the incoming pseudonoise (PN) coded waveform with a locally generated replica at the receiver. It has been previously shown that sequential PN code acquisition schemes have the potential to achieve the best performance, but they are the least analyzed because of the analytical difficulties.

The acquisition time for a PN code acquisition scheme is an important parameter for system design purposes. This thesis investigates the performance of two acquisition schemes in terms of the acquisition time. A fixed sample size (FSS) test and a truncated sequential probability ratio test (TSPRT) are studied with noncoherent demodulation in a classical additive white Gaussian noise (AWGN) channel and in presence of fading. Optimal selection of desired detection and false alarm probabilities, the effects of penalty time, majority logic verification schemes and channel signal to noise ratio (SNR) mismatch problems are thoroughly studied using the flow graph technique. Our results show that the TSPRT is efficient, robust (against fading), fast and suitable for real time low cost implementations.

DTIC QUALITY INSPECTED 8

Accesion For

NTIS CRA&I	☒
DTIC TAB	☐
Unannounced	☐
Justification	

By

Distribution /

Availability Codes

| Dist | Avail and / or Special |

A-1

iii

TABLE OF CONTENTS

LIST OF TABLES

LIST OF FIGURES

ACKNOWLEDGMENT

The author would like to thank to the thesis advisor Professor Alex W., Lam for his continuous support and guidance, and to the second reader Professor Herschel H. Loomis Jr., for his very valuable comments.

I. INTRODUCTION

A. GENERAL

The field of spread-spectrum communications has been around for several decades. Although almost all the applications prior to the 80's fell in the military domain, recent band allocation policies [Ref. 1] and commercially available IC components have made the area appealing to commercial applications as well.

The basic signal characteristics of modern spread-spectrum systems can be defined as follows [Ref. 2].

1. The carrier is an unpredictable, or pseudorandom, wideband signal.

2. The bandwidth of the carrier is much wider than the bandwidth of the data modulation.

3. Reception is accomplished by cross correlation of the received wideband signal with a synchronously generated replica of the wideband carrier.

Spread-spectrum signals provide the following performance attributes [Ref. 3].

1. Low density power-spectra for signal hiding.

2. Interference rejection and anti jam properties.

3. Selective addressing and code division multiple access capability.

4. Message privacy.

5. High resolution and ranging.

1

Spread-spectrum systems can be classified into [Ref. 4] "direct sequence", "frequency hopping", "time hopping", "chirp" and "hybrid systems" with respect to the modulation techniques used in the system.

In direct sequence spread-spectrum systems (DS-SS), spectrum spreading is accomplished by modulating a data modulated signal a second time using a very wideband spreading signal. This second modulating wideband signal is chosen to have properties which facilitate demodulation of the transmitted signal by the intended receiver and make demodulation by an unintended receiver as difficult as possible. This is best accomplished by using a signal that appears random to the unintended receivers and that can be reproduced by deterministic means in the intended receiver. Therefore, this waveform is usually referred as pseudorandom noise (PN) spreading signal.

In a spread-spectrum system using frequency hopping (FH), the carrier frequency is varied pseudorandomly with time, whereas a time hopping (TH) system uses pseudorandom time slots to transmit the signal. Hybrid systems consist of a combination of two or all three of the DS, FH, TH systems. The chirp spread spectrum method can be considered as an analog direct spreading method that does not use a PN code.

B. PN CODE SYNCHRONIZATION

Code synchronization is vital for most spread-spectrum systems, since the PN code is used as a key for spreading and despreading the desired information. Throughout the development of spread-spectrum systems, it is true that [Ref. 3: pp. 214]:

2

More time, effort and money have been spent developing and improving synchronizing techniques than in any other area of spread-spectrum systems. There is no reason to suspect that this will continue to be true in the future.

A complete coverage of the synchronization of spread-spectrum systems can be found in [Ref. 5]. In this thesis, we restrict ourselves to direct sequence spread-spectrum systems.

The data is recovered from a DS-SS communication system by *neutralizing* the effects of the PN sequence that is used for *spreading* the signal at the transmitter's site. This process is termed as *despreading*. Removing the PN sequence from the incoming signal is primarily accomplished by multiplying the incoming signal by a locally generated and phase synchronized replica of the incoming PN sequence. Therefore, a primary function of the receiver is to align the phase of the local replica with the incoming signal's PN sequence. The phase is determined by correlating the two PN sequences. The alignment process is usually accomplished in two stages. The first stage, called *acquisition*, brings the PN sequences into coarse alignment, while the second stage, called *tracking,* brings the PN sequences into precise alignment.

We study noncoherent acquisition of the direct sequence spread-spectrum signals. In this context *noncoherent* refers to the modulating carrier, not the PN sequence. Although coherent systems are simpler and more widely studied, they are not practical because code sequence acquisition is usually performed before recovering the modulating carrier.

Since the acquisition process involves searching through the uncertainty phases of the PN sequence, acquisition schemes can be classified into parallel, serial, and hybrid

schemes with respect to search strategies. The parallel scheme is the fastest search strategy. A parallel scheme inspects all the uncertainty phases simultaneously and decides which is the most likely one. Each uncertainty phase is investigated by a path consisting of a correlator and a matched filter. If the period of the PN sequence is large, the hardware requirement for such a system is excessive and hence is impractical. On the other hand, a serial search scheme inspects one uncertainty phase at a time and determines whether the PN sequences are in alignment. Hardware requirements of such schemes are small, but the complexity of the control process is high and the decision process requires a longer time. Various combinations of the serial and parallel search strategies are also possible.

A serial search acquisition detection scheme that uses a single detector to examine each of the possible waveform alignments for a fixed period of time until the correct one has been located, is termed as a *single dwell* scheme. If the scheme uses cascaded multiple detectors each having a longer examination period than its predecessor to verify the synchronization condition, it is called as a *multiple dwell* scheme. The test terminates if any of the detectors decides a non-synchronization condition. The synchronization condition is accepted if all the detectors decide favorably. In this case the examination time is increased with discrete steps, and since most of the positions will be due to a non-synchronization condition, it is hoped that they will be detected and rejected in earlier stages using a shorter time. These schemes both fall into the category of fixed dwell time or fixed sample size (FSS) schemes. Sequential schemes use a single detector with multiple thresholds, therefore yielding a variable examination time. It has been shown [Ref. 6]

4

that for a two-hypothesis test of a sampled random variable, the sequential probability ratio test (SPRT) is optimum in the sense that for a given false alarm (P_{fa}) and detection (P_d) probability, it requires minimum average number of samples to produce a decision if the samples of the random variable are independent and identically distributed (i.i.d.). Therefore, substantial savings can be achieved on the overall acquisition time using comparable hardware to realize the system where low-cost, fast and reliable acquisition schemes are a necessity, especially in mobile applications [Ref. 1].

This thesis is based on the theory developed in [Ref. 7] and [Ref. 8], two papers which studied the noncoherent sequential acquisition of PN sequences in terms of single search state basis, and the mean acquisition time respectively. These papers served as the original motivation and starting point for this research. In this thesis, we also investigate the variance of the acquisition time, and perform a more detailed acquisition time analysis on the system parameters.

The rest of the thesis is organized as follows. Chapter II presents the PN code acquisition system model and derives the equations to calculate the mean and the variance of the acquisition time using the flow graph technique. Chapter III is devoted to the acquisition time analysis on a single dwell FSS scheme and a truncated sequential probability ratio test (TSPRT) scheme over some important design considerations. Chapter IV examines the performance of both FSS and TSPRT schemes under slowly varying Ricean fading conditions. Finally, the conclusions are given in Chapter V.

II. SYSTEM MODEL AND FLOW GRAPHS

In this chapter, we present the acquisition receiver system model[1] and derive the equations to determine the statistics of the acquisition time using the flow-graph technique developed in [Ref. 9].

A. SYSTEM MODEL

Figure 2.1 depicts a block diagram of the receiver's acquisition system. We assume that there is no data modulation during the acquisition process. The channel is also assumed to have additive white Gaussian noise with two-sided power spectral density $N_0/2$. The input signal at the receiver is

$$r(t) = A_0 a(t + i\Delta T_c)\cos(\omega_0 t + \theta) + n(t) \tag{2.1}$$

where A_0 is the signal amplitude, $a(t)$ is the m-sequence signal waveform with phase $i\Delta T_c$ (i is taken to be an integer without loss of generality), T_c is the chip duration, Δ is the value determining how much the timing of the local PN generator is updated during the acquisition process, ω_0 and θ are the frequency and the phase of the carrier and $n(t)$ is the additive noise. The local replica of the m-sequence has the form $a(t + (j + \gamma)\Delta Tc)$, where j is an integer and $|\gamma| \leq 0.5$. The received signal $r(t)$ is first despread by

---

[1] This chapter, which presents the model and framework to be used in the subsequent chapters, is based on the theory developed in [Ref. 7] and [Ref. 8]. The system model, equations and design approximations, the flow graph of the system model and some of the relevant equations derived from the graphs, and the early termination feature of the coincidence detector were originally propounded in these references. This material is adapted and used with the permission of the authors.

6

cos $(\omega_0 t)$

$\int_{0}^{nT_c} (.)dt$

$X_{i,n}$

$(.)^2$

to tracking

synch.

$r(t)$

Y_n

decision processor

sin $(\omega_0 t)$

$\int_{0}^{nT_c} (.)dt$

$X_{q,n}$

$(.)^2$

$a(t+(j+\gamma)\Delta T_c)$

non-synch.

local PN generator

update phase by ΔT_c
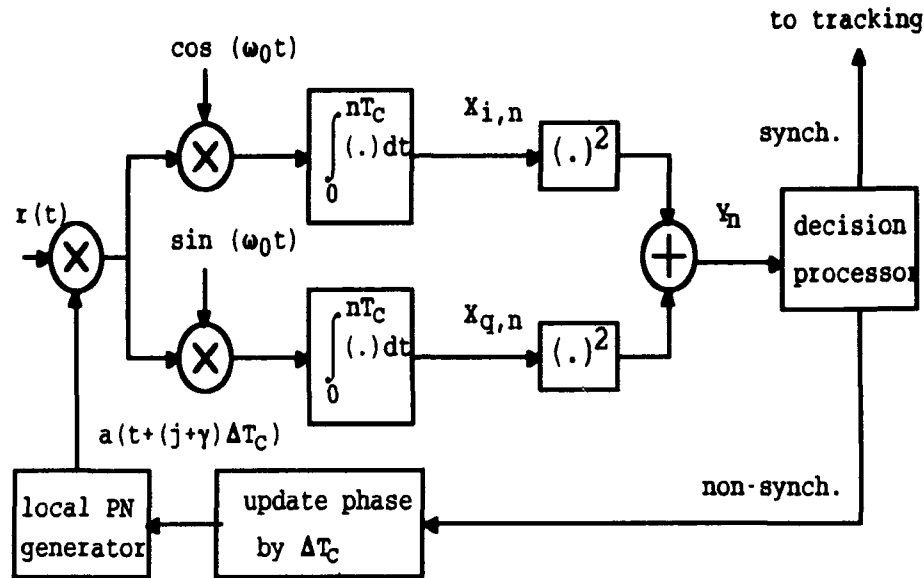
Figure 2.1 Block diagram of noncoherent serial acquisition scheme.

multiplying with the local PN waveform and is then noncoherently demodulated. The test statistics Y_n is used by the decision processor to test if the local and the incoming PN sequences are aligned to within one chip duration. If not, the local PN sequence phase is updated by ΔT_c seconds and the process repeats. If coarse alignment is achieved then i must be equal to j and tracking circuitry takes over to reduce γ to zero. Using the notation in Figure 2.1, after integrating over n chips and ignoring the double frequency terms, the in phase and quadrature components are given by

7

$$X_{i,n} = \int_0^{nT_c} r(t)a(t+(j+\gamma)\Delta T_c)\cos(\omega_0 t)dt = \frac{A_0}{2}T_c S_n\cos\theta + N_{i,n},$$

$$X_{q,n} = \int_0^{nT_c} r(t)a(t+(j+\gamma)\Delta T_c)\sin(\omega_0 t)dt = \frac{A_0}{2}T_c S_n\sin\theta + N_{q,n} \qquad (2.2)$$

respectively, where

$$N_{i,n} = \int_0^{nT_c} n(t)a(t+(j+\gamma)\Delta T_c)\cos(\omega_0 t)dt,$$

$$N_{q,n} = \int_0^{nT_c} n(t)a(t+(j+\gamma)\Delta T_c)\sin(\omega_0 t)dt \qquad (2.3)$$

are independent Gaussian random variables with zero mean and variance $\sigma_n^2 = nT_c N_0/4$.
The expression for S_n is

$$S_n = \frac{1}{T_c}\int_0^{nT_c} a(t+i\Delta T_c)a(t+(j+\gamma)\Delta T_c) \; dt. \qquad (2.4)$$

For a fixed n, $X_{i,n}$ and $X_{q,n}$ are independent Gaussian random variables with variance σ_n^2 and means $(A_0/2)T_c S_n\cos\theta$ and $(A_0/2)T_c S_n\sin\theta$ respectively. Note, however, that $X_{i,n}$ and $X_{i,m}$ are not independent for $n \neq m$, and similarly for $X_{q,n}$ and $X_{q,m}$. The test statistics for deciding alignment or non alignment is

$$Y_n = X_{i,n}^2 + X_{q,n}^2. \qquad (2.5)$$

The random variable Y_n has a non-central Chi-squared probability density function (pdf) with two degrees of freedom, given by

8

$$f_{Y_n}(y_n) = \frac{1}{2\sigma_n^2} e^{-(y_n + \lambda_n)/2\sigma_n^2} I_0(\frac{\sqrt{\lambda_n y_n}}{\sigma_n^2}), \quad y_n \geq 0 \qquad (2.6)$$

where $\lambda_n = [(A_0/2)T_c S_n \cos\theta]^2 + [(A_0/2)T_c S_n \sin\theta]^2 = (A_0^2/4)T_c^2 S_n^2$, and $I_0(.)$ is the modified Bessel function of order zero.

Based on the test statistics Y_n, the decision processor must decide whether the two phases are aligned to within $\Delta T_c/2$ of each other, i.e., $j = i$, or they differ by at least one chip, i.e., $|(j+\gamma) - i|\Delta T_c \geq T_c$. For simplicity, we let $i = 0$. Equivalently, the decision processor has a task of testing the following hypotheses

$$\begin{aligned} H_0 \ (non-alignment) &: \ |j+\gamma| \geq \frac{1}{\Delta} \ and \ |\gamma| \leq \frac{1}{2}, \\ H_1 \ (alignment) &: \ j=i=0 \qquad and \ |\gamma| \leq \frac{1}{2}. \end{aligned} \qquad (2.7)$$

Since $|\gamma| \leq 1/2$, under the hypothesis H_0 we must have $|j| \geq (1/\Delta - 1/2)$. Note that it is possible to have $(1/2) < |j+\gamma| < (1/\Delta)$, which corresponds to neither H_0 nor H_1. It falls between H_0 and H_1.

The parameter λ_n takes on different values under H_0 and H_1. We designate $\lambda_{n,0}$ and $\lambda_{n,1}$ as the worst case values of λ_n under H_0 and H_1 respectively. Using these worst-case parameter values, the likelihood ratio for (2.7) can be written as

$$\Lambda_n(y_n) = \frac{f_{Y_n}(y_n|H_1)}{f_{Y_n}(y_n|H_0)} = \exp(\frac{\lambda_{n,0}-\lambda_{n,1}}{2\sigma_n^2})\frac{I_0(\sqrt{(\lambda_{n,1}/\sigma_n^2)(y_n/\sigma_n^2)})}{I_0(\sqrt{(\lambda_{n,0}/\sigma_n^2)(y_n/\sigma_n^2)})}. \qquad (2.8)$$

We will now derive the nominal worst case values for λ_n, assuming an m-sequence is used as the PN code sequence of communication system in consideration. Denote the

9

chips of the PN sequence by c_k, where $k = \dots, -1, 0, 1, 2, \dots$, and $c_k = \pm 1$. Let $N = 2^m - 1$ be the period of the m-sequence. The PN waveform is

$$a(t) = \sum_{k=-\infty}^{\infty} c_k p_{T_c}(t - kT_c) \qquad (2.9)$$

where $p_{T_c}(t)$ is a rectangular pulse of amplitude 1 and width T_c. Assuming $i = 0$, we obtain an expression for S_n from (2.4) and (2.9) as

$$S_n = \begin{cases} \sum_{k=0}^{n-1} c_k[(1 - |\gamma| \Delta)c_k + (|\gamma| \Delta)c_{k+sgn(\gamma)}] & \text{under } H_1 \\[2mm] \sum_{k=0}^{n-1} c_k[(1 - \delta)c_{k+l} + \delta C_{k+1+l}] & \text{under } H_0 \end{cases} \qquad (2.10)$$

$$= \begin{cases} n(1 - |\gamma| \Delta) + (|\gamma| \Delta) \sum_{k=0}^{n-1} c_k c_{k+sgn(\gamma)} & \equiv S_{n,1} \\[2mm] (1 - \delta) \sum_{k=0}^{n-1} c_k c_{k+l} + \delta \sum_{k=0}^{n-1} c_k c_{k+1+l} & \equiv S_{n,0} \end{cases}$$

where $sgn(x)$ is 1 for $x \geq 0$ and -1 for $x < 0$, $l = \lfloor (j + \gamma) \Delta \rfloor$ and $\delta = (j + \gamma) \Delta - \lfloor (j + \gamma) \Delta \rfloor$. Note that $l \neq 0$ or -1 and $0 \leq \delta < 1$.

Defining the per-chip signal to noise ratio as

$$SNR = \frac{A_0^2 T_c}{2N_0}, \qquad (2.11)$$

we have

10

$$
\frac{\lambda_n}{2\sigma_n^2} = \begin{cases} \frac{1}{n}(SNR)S_{n,1}^2 & \text{under } H_1 \\ \frac{1}{n}(SNR)S_{n,0}^2 & \text{under } H_0 \end{cases} \qquad (2.12)
$$

Since the exact values of $S_{n,o}$ and $S_{n,1}$ are unknown to the receiver in advance, some nominal worst case values must be used in designing the system. Results from simulations for m-sequences suggests that modeling $\sum_{k=0}^{n-1} c_k c_{k+sgn(\gamma)} \approx 0$ under H_1, and

modeling $\sum_{k=0}^{n-1} c_k c_{k+l}$ and $\sum_{k=0}^{n-1} c_k c_{k+1+l} \leq \sqrt{n}$, under H_0 yield the desired results. Using these

approximations we have

$$
\frac{\lambda_n}{2\sigma_n^2} \begin{cases} \approx n(SNR)(1-|\gamma|\Delta)^2 & = \frac{\lambda_{n,1}}{2\sigma_n^2} \text{ under } H_1 \\ \leq SNR & = \frac{\lambda_{n,0}}{2\sigma_n^2} \text{ under } H_0 \end{cases} \qquad (2.13)
$$

These nominal worst case values will be used in the design methods of various acquisition schemes. The design methods for fixed dwell and sequential schemes will be discussed in later chapters.

Regardless of the acquisition scheme, some type of verification logic is usually incorporated in these systems to counter balance the effects of costly false alarms. Here, we employ a majority logic verification scheme such that in case of a *hit*, (deciding H_1 is true) A or less additional tests are performed before committing a final decision. The

11

initial decision will hold if B ($\leq A$) additional tests are favorable; otherwise, it is overturned and the search continues for the next searching state. We also assume that a counter is available and the coincidence detector (CD) employs an early termination mechanism in order to save time. Particularly, the test will be terminated once B favorable tests are accumulated or when there is no chance that B favorable tests can be obtained. Figure 2.2 describes the coincidence detection process with early termination in detail.

B.   FLOW GRAPH OF THE ACQUISITION SCHEME

In [Ref. 9], a flow-graph technique was proposed for determining the statistics of the acquisition time for serial search acquisition schemes. A circular flow-graph was developed using the markovian nature of the underlying serial search acquisition process. We will briefly discuss the technique in the following.

The basic idea behind this technique comes from defining each possible relative position of the phases of the two PN sequences (incoming and local replica) as a state of a discrete markov process. There will be a finite number of states depending the value of the Δ (the parameter which determines how much the phase of the local PN sequence is advanced after each H_0 decision).

Let $p_{ij}(n)$ indicate the probability that the Markov process will move from state i to state j in n steps and let z denote the unit delay operator. The state transition diagram can be mapped into its equivalent flow graph if each transition branch from i to j in the Markovian diagram is assigned a gain equal to $p_{ij}(z)$, where $p_i \triangleq p_{ij}(1)$ is the one-step

12
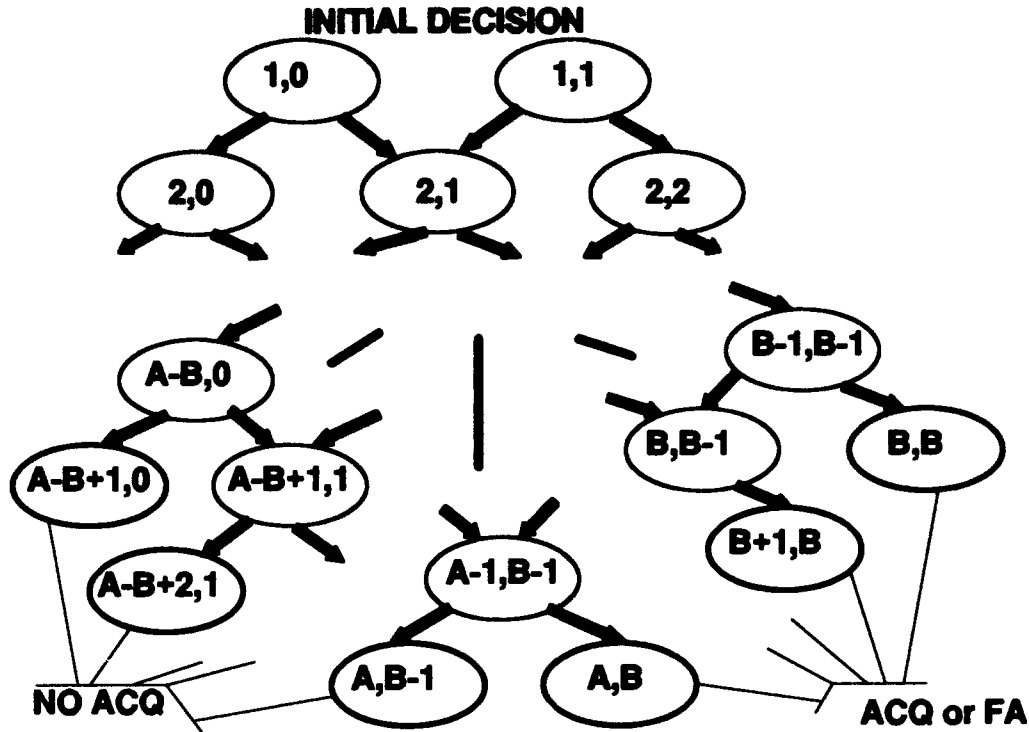
Figure 2.2 Coincidence detection with early termination.

transition probability and z represents the unit delay associated with that transition. The generating function for this transformation is

$$p_{ij}(z) \doteq \sum_{n=o}^{\infty} p_{ij}(n) z^{n}. \qquad (2.14)$$

Note that if the time delay associated with the transitions is specifically t seconds z should be changed to z^t in the above equation. The importance and usefulness of $p_{ij}(z)$ comes from its ability to reveal some statistical information about the underlying process. Using (2.14) one can see that

13

$$\frac{d\, p_{ij}(z)}{dz}\Bigg|_{z=1} = \sum_{n=0}^{\infty} n\, p_{ij}(n) = E\{n\} \qquad (2.15)$$

and higher order moments can be similarly obtained.

Figures 2.3 and 2.4 show a general and a detailed version of the circular flow-graph diagram for the system model presented in the previous section. This graph has a total of $\nu+2$ states. Two of these states are the acquisition state and the false-alarm state, where the former is absorbing and the latter is not. The remaining $\nu=N/\Delta$ states are searching states, where N is the PN code sequence period and Δ (taken to be 1/2 for this system) is the fraction of a chip to be updated each time an H_0 decision is made. We assume that the code tracking loop following the acquisition circuit can successfully track the incoming code phase if the phase offset is smaller than T_c seconds. If we set $\gamma=1/2$, where γT_c is the timing difference between the incoming and the locally generated PN waveforms when $j=i$, then a total of four states will correspond to H_1(alignment hypothesis) as shown in Figure 2.4. The number of search states under H_0 is a ν-4 or namely $2N$-4.

The search for the acquisition could start in any of the searching states, regarding to the initial phase of the incoming PN sequence. Therefore, the initial starting state is assumed to have some *a priori* distribution, which reflects the designers confidence about the initial relative position of the codes.
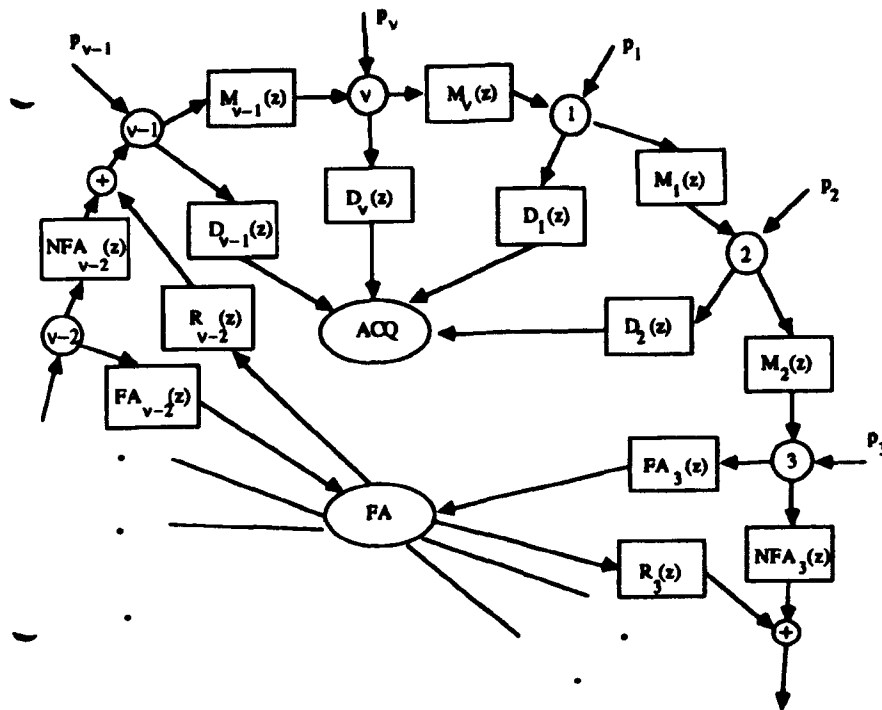
Figure 2.3 General circular flow-graph diagram.
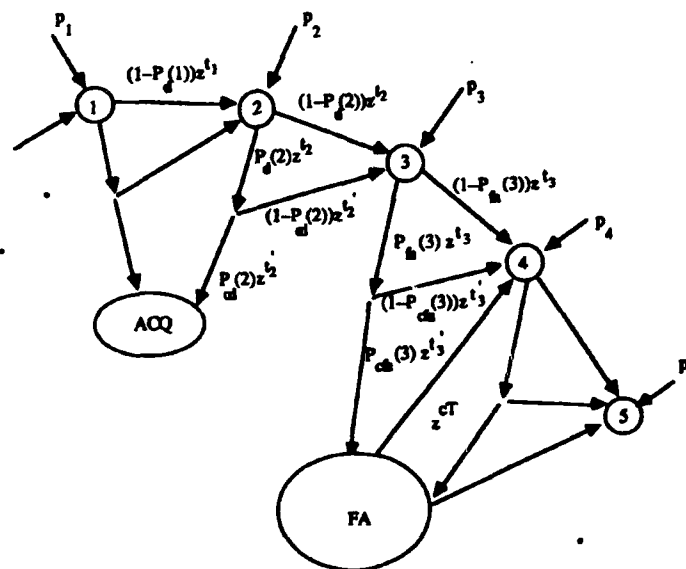
Figure 2.4 Detailed flow-graph diagram.

15

C. EXPECTED RESULTS

Prior to making a more detailed analysis this section deals with a theoretical best case situation to reveal the relationships between important parameters for a serial search acquisition scheme.

Consider the circular flow-graph diagram of Figure 2.3. Let P_d indicate the probability that the system will reach acquisition while the codes are in any of the H_1 states and P_{fa} denote the probability of committing an acquisition decision while the codes are in any H_0 states. It is easy to see that $P_d = 1.0$ and $P_{fa} = 0.0$ is the best case for this system. Let M_{ss} denote the sample size, i.e., the number of chips to be integrated prior to committing a decision. Since the codes may take any initial relative phase, e.g., as would be for an arbitrary asynchronous communication scheme, we assume a uniform initial state prior probability distribution. This system will reach the acquisition state as soon as a search state under H_1 is reached and will never circle more than once, so we expect to see the least possible mean time to acquire with the least variance. It is easy to see that the only randomness for the system is due to prior starting state probability distribution and the mean and variance of the acquisition time will heavily depend on this distribution. The mean time to acquire is

$$
\begin{aligned}
\overset{\bullet}{\mu}_{TACQ} &= \sum_{i=1}^{v} P_i \, T_{i,acq} = \frac{T_c}{2N} \left(\sum_{i=3}^{2N-2} (2N-i)M_{ss} + 4M_{ss} \right) \\
&= T_c M_{ss} \left(N - \frac{5}{2} + \frac{6}{N} \right) \\
&\approx M_{ss} (NT_c) = M_{ss} \, T
\end{aligned}
\tag{2.16}
$$

where $T = NT_c$ is the data bit period and N is the PN code sequence length.

16

Following a similar derivation for the variance and using $\mu^{*}_{TACQ} = M_{ss}NT_c$ for simplicity, we obtain

$$\sigma^{2*}_{TACQ} = \sum_{i=1}^{v} P_i (T_{i,ACQ} - \mu^{*}_{TACQ})^2 = \frac{T_c^2}{2N} \left(\sum_{i=3}^{2N-2} [(2N-i)NM_{ss} - NM_{ss}]^2 + 4(M_{ss} - NM_{ss})^2 \right)$$

$$= T_c^2 M_{ss}^2 \left(\frac{N^2}{3} - \frac{7}{6} \right)$$

$$\approx \frac{1}{3} M_{ss}^2 (NT_c)^2 = \frac{1}{3} M_{ss}^2 T^2.$$

$$(2.17)$$

Note that definite detection and no false alarm assumption is unrealistic and will not happen in nature. Nevertheless, this simplistic approach provides some important aspects of the total system.

We can see that we will have an absolute lower bound due to uncertainty of the phase of the incoming PN sequence. For this lower bound the sample size constitutes a key parameter, the mean acquisition time will be basicly dependent upon the sample size and the variance will be proportional to the square of the sample size. In realistic cases the false alarms and misses will prolong the average acquisition time and increase the variance. Since the states under H_0 largely outnumbers the states under H_1, H_0 states will be dominant in mean and variance calculations.

The next logical question to ask is how the actual detection and false alarm probabilities would effect our performance parameters. The following sections will provide a more detailed exact analysis for the overall system performance and seek optimal design parameters.

D. MEAN AND VARIANCE OF THE ACQUISITION TIME

1. General

The flow-graph diagram depicted in Figure 2.3 provides us a technique of obtaining first and higher order statistics of the acquisition time. We are interested in finding the gain function $P_{acq}(z)$, where

$$P_{acq}(z) = \sum_{i=1}^{v} p_i \, P_{i,acq}(z) \qquad (2.18)$$

with $P_{i,acq}(z)$ denoting the gain function going from state i to the acquisition state ACQ. We assume a uniform *a priori* initial phase distribution, i.e., $p_i = 1/v = 1/2N$. The individual gain functions from states can be found as

$$
\begin{aligned}
P_{v-1,acq}(z) &= \frac{(D_{v-1} + M_{v-1}D_v + M_{v-1}M_vD_1 + M_{v-1}M_vM_1D_2)(z)}{1 - M_1M_2M_3...M_v(z)}, \\
P_{v-2,acq}(z) &= M_{v-2}P_{v-1,acq}(z), \\
&\quad\cdots\cdots \\
&\quad\cdots\cdots \\
P_{4,acq}(z) &= M_4M_5M_6...M_{v-2}P_{v-1,acq}(z), \\
P_{3,acq}(z) &= M_3M_4M_5...M_{v-2}P_{v-1,acq}(z), \\
P_{2,acq}(z) &= D_2 + M_2P_{3,acq}(z), \\
P_{1,acq}(z) &= D_1 + M_1P_{2,acq}(z), \\
P_{v,acq}(z) &= D_v + M_vP_{1,acq}(z).
\end{aligned}
\qquad (2.19)
$$

Note that these functions can be written in various ways since we are dealing with a circular graph structure. It is possible to write all the other states in terms of any single one of them. The form presented above expresses all states either explicitly or implicitly in terms of $P_{v-1,acq}(z)$, the state which intuitively has the least expected time to acquire and is chosen to provide computational simplicity. For the states under H_1, $M(z)$

18

stands for the *miss* gain function and $D(z)$ stands for the *detection* gain function, whereas $M_3 \ldots\ldots M_{\nu-2}(z)$ denotes the process *gain* functions for the states under H_0. Next we can find the individual gain functions as follows:

$$
\begin{aligned}
M_{\nu-1}(z) &= (1-P_d(\nu-1))z^{t_{\nu-1}} + P_d(\nu-1)(1-P_{cd}(\nu-1)z^{t_{\nu-1}+t'_{\nu-1}}, \\
D_{\nu-1}(z) &= P_d(\nu-1)P_{cd}(\nu-1)z^{t_{\nu-1}+t'_{\nu-1}} \\
&= 1 \quad - \quad M_{\nu-1}(z)
\end{aligned}
\tag{2.20}
$$

where $P_d(\nu\text{-}1)$ is the *detection* probability and $P_{cd}(\nu\text{-}1)$ is the *coincidence* detector detection probability for state $\nu - 1$. The time delay $t'_{\nu-1}$ is the sum of A or less delay terms depending on whether an early terminatible coincidence detection scheme is used or not. In case of early termination feature it can be expressed as

$$
\begin{aligned}
t'_{\nu-1} &= \sum_{j=0}^{A-B} \begin{bmatrix} A-j-1 \\ B-1 \end{bmatrix} (1-P_d(\nu-1))^{A-j-B}(P_d(\nu-1))^B(A-j)t_{\nu-1} \\
&+ \sum_{j=0}^{B-1} \begin{bmatrix} A-B+j \\ j \end{bmatrix} (1-P_d(\nu-1))^{A-B+1}(P_d(\nu-1))^j(A-B+1+j)t_{\nu-1}.
\end{aligned}
\tag{2.21}
$$

This equation can be verified by examining the early-termination coincidence detection process described in Figure 2.2. Assuming the coincidence tests are statistically independent, the early termination procedure does not affect the coincidence detection probability which has a binomial distribution in both cases. It can be written as

19

$$P_{cd}(\nu-1) = \sum_{j=B}^{A} \begin{bmatrix} A \\ j \end{bmatrix} (1 - P_d(\nu-1))^{A-j}(P_d(\nu-1))^j. \qquad (2.22)$$

Note that the individual gain functions for the other H_1 states can be found with a simple substitution of the indices. For the remaining of the search states under H_0 we can write

$$M_3(z) = NFA_3(z) + FA_3(z) \, R_3(z) \qquad (2.23)$$

where

$$
\begin{aligned}
NFA_3(z) &= (1-P_{fa}(3))z^{t_3} + P_{fa}(3)(1-P_{cfa}(3))z^{t_3+t_3'}, \\
FA_3(z) &= P_{fa}(3)P_{cfa}(3)z^{t_3+t_3'} = 1 - NFA_3(z), \\
R_3(z) &= z^{cNT_c}.
\end{aligned}
\qquad (2.24)
$$

In the above equations $FA_3(z)$ and $NFA_3(z)$ are the gain functions for the false-alarm and correct dismissal respectively and $R_3(z)$ is the return gain function for state 3, which specify the penalty time incurred in returning from the FA state. The constant c is the number of bit intervals elapsed before returning from false alarm state. Again the gain functions for states $4,5,6,\dots,\nu-2$ can be found with straightforward substitution of the indices, whereas the coincidence false alarm probabilities and time delays can be found from the equations (2.21) and (2.22) by substituting P_d with P_{fa}.

So far all the necessary elements constituting the overall gain function, $P_{acq}(z)$ are determined. A simple verification of the equations can be obtained by evaluating $P_{acq}(1)$, which equals to unity because the ACQ state is the only absorbing state in this system.

Following the steps outlined in [Ref. 9], the mean and the variance of the acquisition time can be readily obtained by using the formulas

$$
\mu_{TACQ} = \frac{dP_{acq}(z)}{dz} \Bigg|_{z=1} ,
$$

$$
\sigma^2_{TACQ} = \left[\frac{d^2 P_{acq}(z)}{dz^2} + \frac{dP_{acq}(z)}{dz} - \left(\frac{dP_{acq}(z)}{dz} \right)^2 \right]_{z=1} .
$$

(2.25)

2. The Mean Acquisition Time

Now we will carry out some algebra starting from the overall gain function $P_{acq}(z)$ of equation (2.19). The following symmetry conditions always hold if complete random sequences were used. They are also valid for m-sequences with long periods.

$$
\begin{aligned}
M_{d1}(z) &\triangleq M_{\nu}(z) = M_1(z) \\
M_{d2}(z) &\triangleq M_{\nu-1}(z) = M_2(z) \\
D_{d1}(z) &\triangleq D_{\nu}(z) = D_1(z) \\
D_{d2}(z) &\triangleq D_{\nu-1}(z) = D_2(z) \\
M_{fa}(z) &\triangleq M_3(z) = M_4(z) = \ldots = M_{\nu-2}(z)
\end{aligned}
$$

(2.26)

Note also, with ACQ being the only absorbing state $P_i(1) = 1.0$, $i=1,\ldots,\nu$ and $M_{fa}(1) = 1.0$. Using these results and carrying out the algebra we can write

$$
\begin{aligned}
P'_{3,acq}(1) &= (\nu-4)M'_{fa}(1) + P'_{\nu-1,acq}(1), \\
P'_{2,acq}(1) &= D'_{d2}(1) + M'_{d2}(1) + M_{d2}(1)P'_{3,acq}(1), \\
P'_{1,acq}(1) &= D'_{d1}(1) + M'_{d1}(1) + M_{d1}(1)P'_{2,acq}(1), \\
P'_{\nu,acq}(1) &= D'_{d1}(1) + M'_{d1}(1) + M_{d1}(1)P'_{1,acq}(1)
\end{aligned}
$$

(2.27)

where

21

$$M'_{d1}(1) = (1 - P_{d1})t_{d1} + P_{d1}(1 - P_{cd1})(t_{d1} + t'_{d1}),$$

$$D'_{d1}(1) = P_{d1}P_{cd1}(t_{d1} + t'_{d1}),$$

(2.28)

and $M'_{d2}(1)$ and $D'_{d2}(1)$ follows with an indices substitution.

The other states under H_0 can be similarly found as below,

$$P'_{i,acq}(1) = (v - i - 1)M'_{fa}(1) + P'_{v-1,acq}(1) \ , \quad i = 4,5,...,v-2$$

(2.29)

where

$$M'_{fa}(1) = t_{fa} + t'_{fa}P_{fa} + cNT_cP_{fa}P_{cfa}.$$

(2.30)

Finally for the state v-1 we can write

$$
\begin{aligned}
P'_{v-1,acq}(1) &= \frac{D'_{d1}(1)}{1 - M_{d1}^{2}M_{d2}^{2}(1)}(M_{d2} + M_{d1}M_{d2})(1) + \frac{D'_{d2}(1)}{1 - M_{d1}^{2}M_{d2}^{2}(1)}(1 + M_{d1}D_{d1} + M_{d1}^{2}M_{d2})(1) \\
&+ \frac{M'_{d1}(1)}{1 - M_{d1}^{2}M_{d2}^{2}(1)}(M_{d2}D_{d1} + M_{d1}M_{d2}D_{d2})(1) + \frac{M'_{d2}(1)}{1 - M_{d1}^{2}M_{d2}^{2}(1)}(D_{d1} + M_{d1}D_{d1} + M_{d1}^{2}D_{d2})(1) \\
&+ \frac{M'_{d1}(1)}{(1 - M_{d1}^{2}M_{d2}^{2}(1))^2}(2M_{d1}M_{d2}^{2}D_{d2} + 2M_{d1}M_{d2}^{3}D_{d1} + 2M_{d1}^{2}M_{d2}^{3}D_{d1} \\
&\quad\quad\quad + 2M_{d1}^{3}M_{d2}^{3}D_{d2})(1) \\
&+ \frac{M'_{d2}(1)}{(1 - M_{d1}^{2}M_{d2}^{2}(1))^2}(2M_{d1}^{2}M_{d2}D_{d2} + 2M_{d1}^{2}M_{d2}^{2}D_{d1} \\
&\quad\quad\quad + 2M_{d1}^{3}M_{d2}^{2}D_{d1} + 2M_{d1}^{4}M_{d2}^{2}D_{d2})(1) \\
&+ \frac{M'_{fa}(v-4)}{(1 - M_{d1}^{2}M_{d2}^{2}(1))^2}(M_{d1}^{2}M_{d2}^{2}D_{d2} + M_{d1}^{2}M_{d2}^{3}D_{d1} \\
&\quad\quad\quad + M_{d1}^{3}M_{d2}^{3}D_{d1} + M_{d1}^{4}M_{d2}^{3}D_{d2})(1).
\end{aligned}
$$

(2.31)

After replacing v by 2N, the expression for the mean acquisition time for our system can be written in the following form

$$\mu_{TACQ} = \sum_{i=1}^{\nu} p_i P'_{i,acq}(1)$$

$$= \frac{1}{2N}[(2N^2-7N+6)M'_{fa}(1)+(2N-3)P'_{\nu-1,acq}(1)+P'_{1,acq}(1)$$

$$+ P'_{2,acq}(1)+P'_{\nu,acq}(1)].$$

(2.32)

3. The Variance of The Acquisition Time

Equation (2.25) depicts that an expression for the variance can be obtained by taking the second derivative of $P_{acq}(z)$. Using the same symmetry conditions shown in equation (2.26) we can write

$$P''_{3,acq}(1) = ((\nu-4)M''_{fa} + (\nu-4)(\nu-5)(M'_{fa})^2$$
$$+ (2\nu-8)M'_{fa}P'_{\nu-1,acq} + P''_{\nu-1,acq})(1),$$

$$P''_{2,acq}(1) = (D''_{d2} + M''_{d2} + 2M'_{d2}P'_{3,acq} + M_{d2}P''_{3,acq})(1),$$

$$P''_{1,acq}(1) = (D''_{d1} + M''_{d1} + 2M'_{d1}P'_{2,acq} + M_{d1}P''_{2,acq})(1),$$

$$P''_{\nu,acq}(1) = (D''_{d1} + M''_{d1} + 2M'_{d1}P'_{1,acq} + M_{d1}P''_{1,acq})(1),$$

(2.33)

and for the other states under H_0

$$P''_{i,acq}(1) = ((\nu-i-1)M''_{fa} + (\nu-i-1)(\nu-i-2)(M'_{fa})^2$$
$$+ 2(\nu-i-1)M'_{fa}P'_{\nu,1,acq} + P''_{\nu-1,acq})(1), \quad i = 4,5,\dots,\nu-2.$$

(2.34)

The gain function $P_{\nu-1,acq}(z)$ has the form $A(z)/B(z)$ and can be differentiated using normal techniques.

$$P''_{\nu-1,acq}(1) = \frac{A''(1)}{B(1)} - \frac{2B'(1)P'_{\nu-1,acq}(1)}{B(1)} - \frac{A(1)B''(1)}{B^2(1)}$$

(2.35)

where

23

$$A(z) = D_{d2}(z) + M_{d2}(z)D_{d1}(z) + M_{d2}(z)M_{d1}(z)D_{d1}(z) + M_{d2}(z)M_{d1}^2(z)D_{d2}(z),$$

$$B(z) = 1 - M_{d1}^2(z)M_{d2}^2(z)M_{fa}^{r-4}(z).$$

(2.36)

The rest follows with a tedious but simple bookkeeping exercise. The resulting equations which will be used to calculate the variance of the acquisition time are rather messy and we do not show them here, but they can be easily put in a computer program and an acquisition time analysis may follow.

III. ACQUISITION TIME ANALYSIS

A. INTRODUCTION

The *decision processor* of the DS-SS receiver depicted in Figure 2.1 has the task of resolving between the hypotheses given by equation (2.7). This task will be accomplished using the test statistics Y_n. The decision processor[2] can be implemented in various schemes based on the likelihood ratio of equation (2.8).

In this chapter, we will study three decision schemes: *a fixed sample size (FSS) test* scheme, a *sequential probability ratio test (SPRT)* scheme and a *truncated SPRT* scheme. These schemes are previously studied in [Ref. 7] and [Ref. 10] for a single search state cell basis to obtain the average test lengths for *SPRT* and *TSPRT* and comparing them to that of the *FSS* test. The *flow-graph* technique presented in previous chapter is applicable to the all decision schemes using a serial search algorithm, hence can be adequately used to study some important design considerations in terms of the performance parameters, namely the *mean* and the *variance* of the acquisition time.

B. FIXED SAMPLE SIZE SCHEME

In a fixed sample size (FSS) decision scheme, the length of integration is fixed and a decision is made based on the resulting test statistics, Y_n. If the integration length is taken as from $t = 0$ to $t = MT_c$, the test can be described by

---

[2] The decision processor design methods discussed in this chapter are adapted from [Ref. 7].

$$\Lambda_M(y_M) \begin{cases} \geq \tau & say \; H_1 \\ < \tau & say \; H_0 \end{cases} \tag{3.1}$$

where τ is the threshold. Since the likelihood ratio of equation (2.8) is a monotonically increasing function of the variable y_n, equivalently the test can be written as

$$y_M \begin{cases} \geq \tau' = \Lambda_M^{-1}(\tau) & say \; H_1 \\ \\ < \tau' = \Lambda_M^{-1}(\tau) & say \; H_0 \end{cases} \tag{3.2}$$

where $\Lambda_n^{-1}(.)$ is the inverse function of $\Lambda_n(.)$ of equation (2.8).

The cumulative distribution function (cdf) of Y_n can be written in terms of the Marcum Q function as

$$F_{Y_n}(y_n) = P(Y_n \leq y_n) = 1 - Q(\sqrt{\frac{\lambda_n}{\sigma_n^2}}, \sqrt{\frac{y_n}{\sigma_n^2}}), \quad y_n \geq 0 \tag{3.3}$$

where the Q function is defined as [Ref. 11]

$$Q(\zeta,\xi) = \int_\xi^\infty x \; e^{-(x^2+\zeta^2)/2} I_0(\zeta x) \; dx. \tag{3.4}$$

An iterative algorithm for calculating the Q function can be found in [Ref. 12].

1. Design of Decision Parameters

Using equation (3.3) we can write the false alarm and the miss probabilities

for the FSS test as

$$P_{fa} = Q(\sqrt{\frac{\lambda_{M,0}}{\sigma_M^2}} \ , \ \sqrt{\frac{\tau'}{\sigma_M^2}}),$$

$$P_{miss} = 1 - Q(\sqrt{\frac{\lambda_{M,1}}{\sigma_M^2}} \ , \ \sqrt{\frac{\tau'}{\sigma_M^2}}).$$

(3.5)

From these equations, the values of τ' and M can be obtained by iteratively solving

the equations simultaneously, such that $P_{fa} \leq \alpha$ and $P_{miss} \leq 1 - \beta$, where α and β are

the desired false alarm and detection probabilities respectively.

The nominal worst case values of (λ_n/σ_n^2) are derived in Chapter II by equation

(2.13) and repeated below.

$$\frac{\lambda_n}{2\sigma_n^2} \begin{cases} \approx n(SNR)(1-|\gamma|\Delta)^2 = \dfrac{\lambda_{n,1}}{2\sigma_n^2} \ under \ H_1 \\[4mm] \approx SNR = \dfrac{\lambda_{n,0}}{2\sigma_n^2} \ under \ H_0 \end{cases}$$

(3.6)

Considering the structure of flow graph depicted in Figure 2.3 of Chapter II we

will need the $(\lambda_n/2\sigma_n^2)$ ratio for the case of $|j+\gamma| = 1.5$. Recall from equation (2.7)

that for $|j+\gamma| \leq .5$ we have the hypothesis H_1 and for $|j+\gamma| \geq 2.0$ we have the

hypothesis H_0. Therefore $(\lambda_n/2\sigma_n^2)$ ratio for $|j+\gamma| = 1.5$, denoted by $(\lambda_{n,1/2}/2\sigma_n^2)$ can

be approximated by

27

$$\frac{\lambda_{n,1/2}}{2\sigma_n^2} = \frac{1}{3}\frac{\lambda_{n,1}}{2\sigma_n^2} + \frac{2}{3}\frac{\lambda_{n,0}}{2\sigma_n^2} \qquad (3.7)$$

using a first order linear approximation.

2.   Mean and Variance Analysis of The FSS Scheme

We are now ready to use the expressions derived for the mean and variance of the acquisition time. Note that the required parameters are $P_{d1} \geq \beta$, $P_{fa} = \alpha$, all the time delays for initial tests are MT_c and the time delays for coincidence tests can be calculated using equation (2.21). Finally,

$$P_{d2} = Q\left(\sqrt{\frac{\lambda_{M,1/2}}{\sigma_M^2}}, \sqrt{\frac{\tau'}{\sigma_M^2}}\right). \qquad (3.8)$$

a.   Optimal Choices of The Design Parameters

We have seen that specifying the desired false alarm and detection probabilities suffices to design a *FSS* decision scheme. In previous studies these parameters are forced to be arbitrarily chosen obeying the intuition that α should be reasonably close to zero while β should be reasonably close to unity. Knowledge of the mean and the variance of the resulting acquisition time provides us a means of optimal selection of these parameters with respect to these performance parameters.

Unfortunately, equation (3.5) depicts that α and β are related with the design parameters, the sample size and the threshold in terms of *Marcum Q* function. The values of interest does not allow us to make the well known exponential

28

approximations of the *Marcum Q* function, hence we have to depend on the numerical results rather than a more desirable rigorous analytical analysis.

Our argument will now continue with the illustration of some examples. As the first example we employ a FSS, PN code serial search acquisition scheme with an early terminatable coincidence detector. Using the notation of Chapter II we assume $\gamma = .5$, $\Delta = .5$ for this system. The coincidence detector parameters are $A = 4$ and $B = 2$. The design chip *SNR* = -10 dB and the amount of time elapsed for returning from the *FA* states (penalty time) is set to be 5 bit periods.

Figures 3.1 and 3.2 show the graphs for normalized μ_{TACQ} and σ^2_{TACQ} versus various values of desired false alarm (α) and detection (β) probabilities for this system respectively. The plots have the following common properties:

- The rate of the change of the values of with α are much greater than the variations due to β.

- Both curves has a minimum point for a certain α and β combinations.

The minimum μ_{TACQ} is 111.46 T and occurs at $\alpha = .06$, $\beta = .69$, whereas the minimum σ^2_{TACQ} is 6.0e3 T^2 and occurs at $\alpha = .06$, $\beta = .8$.

Let us consider the case of minimum μ_{TACQ} and carry out a simple comparison with the theoretical values computed in Section C of Chapter II. The fixed sample size, M_{fss} calculated by equation (3.5) for these values of α and β is 70, and recall from equation (2.17) that 70 bit periods is the lowest mean time to acquire if it were possible to achieve definite detection and no false alarm hypothesis with this sample size value. On the other hand, the real values are $P_{d1} = 0.6967$, $P_{d2} = 0.2846$, $P_{fa} = 0.06$,

29

the *coincidence* test detection and false alarm probabilities from equation (2.22) are $P_{cd1} = 0.9138$, $P_{cd2} = 0.3213$ and $P_{cfa} = 0.0199$. The coincidence detector time delays from equation (2.21) are $t_{d1}' = 189.5$, $t_{d2}' = 234.9$ and $t_{fa}' = 220.8$ chip periods. The effective sample size per state, i.e., $M_{fa}'(1)$, for H_0 states can be calculated using equation (2.30) to be 89.36. Therefore, considering a $P_{fa} = 0.06$, the system would have reached acquisition on the average 89.36 bit periods if it were quaranteed to acquire as soon as it reaches a state under H_1. However, the actual mean acquisition time came out to be 111.46 bit periods. H_1 states and additional sweeps of the uncertainty region prolonged the mean acquisition time to 111.46, only 22.1 bit periods. As we remarked earlier the states under H_0 dominates the resulting mean and variance of the acquisition time. This simple example and the greater rate of change with respect to α verifies this hypothesis.

Surprisingly, we observe that the desired *detection* probability, β which minimizes either the mean or the variance of the acquisition time, takes moderate values, opposing the intuitive thought that it should be as close to unity as possible. We will explain this phenomenon by stressing the importance of the *sample size* per decision. We have seen in Section C of Chapter II that the average acquisition time heavily depend on the sample size. Therefore, it should be kept as low as possible to minimize the acquisition time. For a fixed dwell acquisition scheme such as FSS, the sample size per decision is fixed a priori and we denote it M_{fss}. The plot of the M_{fss} versus α and β is given in Figure 3.3.
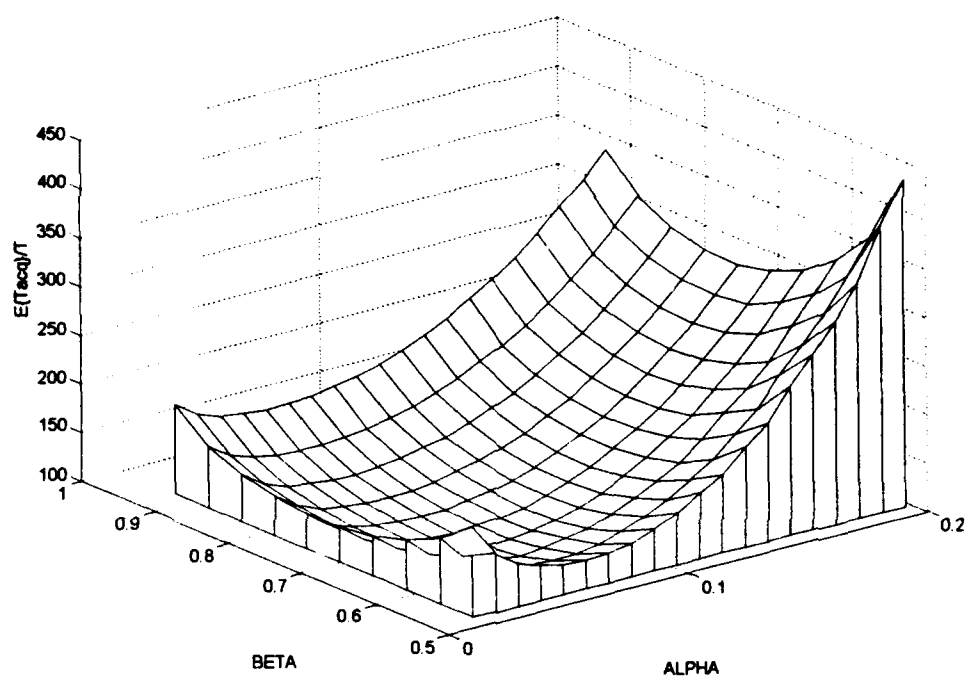
Figure 3.1 Average acquisition time for various α and β combinations.
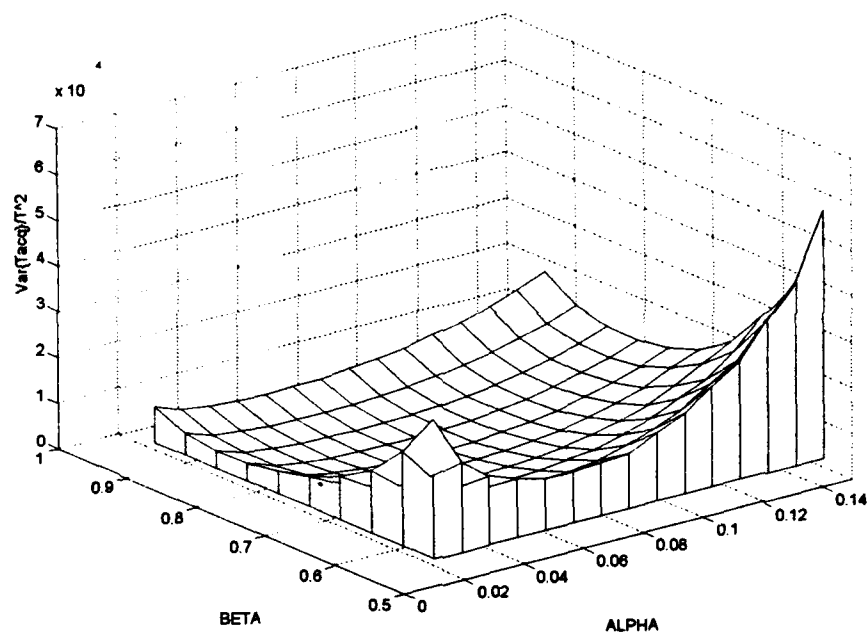
Figure 3.2 Variance of the acquisition time for various α and β combinations.

31
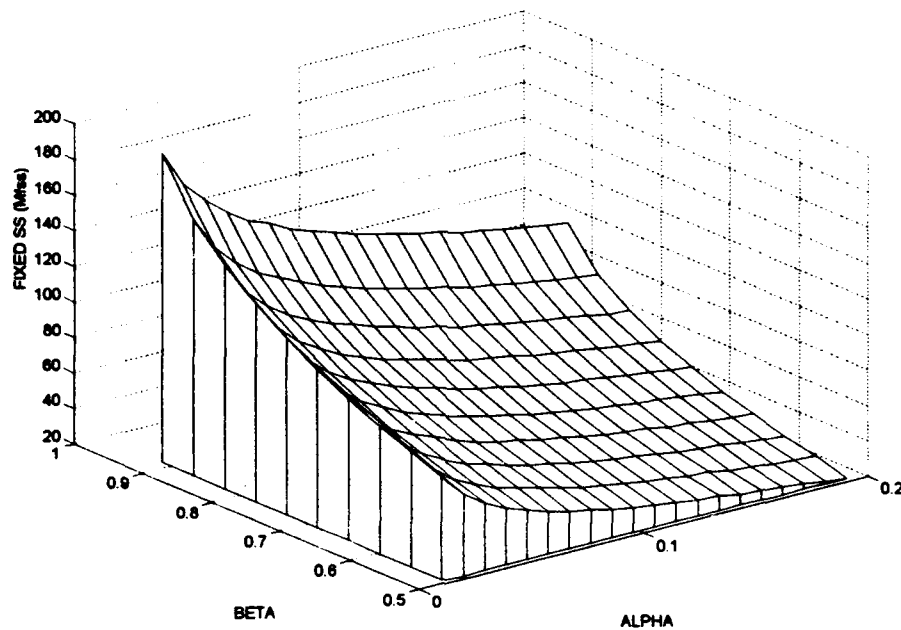
Figure 3.3 The fixed sample size (Mfss) versus various α and β combinations.

This graph has an interesting property that along the main diagonal the values are "almost" symmetrical, that is, for a fixed α, M_{fss} increases exponentially with increasing β, and for a fixed β decreasing α has "almost" the same effect. In fact the rate of change with respect to β is slightly greater. Choosing a small α and large β, requires a large M_{fss} which in turn results in a large mean and variance of the acquisition time. Otherwise, false alarms and additional sweeps of the uncertainty region increase the same parameters. Therefore, an optimum acquisition time can be achieved in terms of the design parameters α and β. Since the states under H_0 bear far more weight than the states under H_1 and false alarms are costly, minimal α turns out to be a small value (close to zero), while selecting a large β increases the M_{fss} excessively with respect to its contribution, minimal β takes moderate values.

The second example is chosen to illustrate the potential benefits of using a coincidence detector in the acquisition system. The only difference is that we have set the values of A and B both to be zero, and therefore no coincidence detector is used. The minimum value of the average acquisition time is now increased to 171.9877 T for the values of $\alpha=0.0046$, $\beta=0.63$. The minimum value of the variance is also increased to 13702 T^2 for $\alpha = 0.0051$, $\beta = 0.79$.

Our argument for the design parameters completely fit in this system as well. Note that minimal α turns out to be approximately 10 times smaller than the previous example, because coincidence detector by design decreases the effective false alarm probability. We will investigate this matter further in detail.

Our discussion so far targeted the two performance parameters, i.e., the mean and the variance of the acquisition time separately. We have seen from the examples that both parameters are minimized by close but distinct choices of design parameters α and β and yet no suggestion has been made which pair should be used in the design. Before further discussion, we summarize our results for the design examples in Table 3.1.

The *Tchebycheff Inequality* [Ref. 13] is a well known theorem of probability theory and is a measure of the concentration of an RV near its mean η and its variance σ^2. It can be formulated as

$$P\{|x-\eta| \geq \varepsilon\} \leq \frac{\sigma^2}{\varepsilon^2} \qquad ,\forall\ \varepsilon > 0. \qquad (3.9)$$

TABLE 3.1 The system values for the design examples of FSS test.

	Minimum μ_{TACQ} Parameters			Minimum σ^2_{TACQ} Parameters		
	(α,β)	μ_{TACQ}	σ^2_{TACQ}	(α,β)	μ_{TACQ}	σ^2_{TACQ}
System with ETCD	(0.06, 0.69)	111.46	7014.0	(0.06, 0.80)	119.08	6002.0
System with No CD	(0.0046, 0.63)	171.99	16572.0	(0.0051, 0.79)	183.63	13702.0

The proof of this theorem is simple and can be found in [Ref. 13]. Note that even the bound in (3.9) is shown to be not so tight for specific densities, i.e., normal densities, we could still use it conceptually to find a criteria for choosing optimal design parameters.

We remark that the probability density function of the acquisition time be positive definite, that is $T_{ACQ} > 0$. We are interested in finding an upper bound for the probability for the cases T_{ACQ} is greater than μ_{TACQ} up to several order of magnitude. Let T_{max} denote the maximum "acceptable" acquisition time for a system of this nature. Setting $\varepsilon = T_{max} - \mu_{TACQ}$ in (3.9), we obtain

$$P\{t_{ACQ} \geq T_{max}\} \leq P\{|t_{ACQ} - \mu_{TACQ}| \geq T_{max} - \mu_{TACQ}\} \leq \frac{\sigma^2_{TACQ}}{(T_{max} - \mu_{TACQ})^2}. \qquad (3.10)$$

To clarify a possible ambiguity, the reader should note that we are not actually interested in determining the probability that the system will reach acquisition

in less than T_{max} seconds, although equation (3.10) depicts a pessimistic and quite possibly a loose bound for this probability. The usefulness of the *Thebycheff's Inequality* comes from the fact that it can be used for any random variable if the first and second order statistics are known. Therefore, it can be adequately used for our case, to make an even comparison between the multiple choices with which we are confronted and to help us to narrow our attention to a unified direction.

The right-most expression in (3.10) is the bound for the upper tail probability which we want to minimize. To be consistent with the notation we have been using, we will denote the parameters that minimizes the right-most expression using an asterisk (*) following the relevant parameter to demonstrate that the parameter is "optimal" in this context. The numerical results for various T_{max} suggests the α^* and β^* combinations lay between the cases of minimum μ_{TACQ} and minimum σ^2_{TACQ}. In fact it is easy to see from equation (3.10) that for the case of $T_{max} \gg \mu_{TACQ}$ minimum σ^2_{TACQ} choices minimize the right-most expression in (3.10). Figure 3.4 depicts this behavior of α^* and β^* graphically for the design examples of this section from Table 3.1. System 1 corresponds to the design example which uses an early terminatable coincidence detector, whereas system 2 is the example without the coincidence detector in this figure. The x - axis assumes various values of T_{max}/T normalized by the sequence length N. Note that α^* values remain essentially unchanged for the entire range, which verifies our earlier observation about the dominance of the H_0 states. Figure 3.5 shows the corresponding values of the normalized μ^*_{TACQ} and σ^{2*}_{TACQ} of the same examples for the same range of T_{max}/NT. Note that as T_{max} increases μ^*_{TACQ} values increase and σ^{2*}_{TACQ}

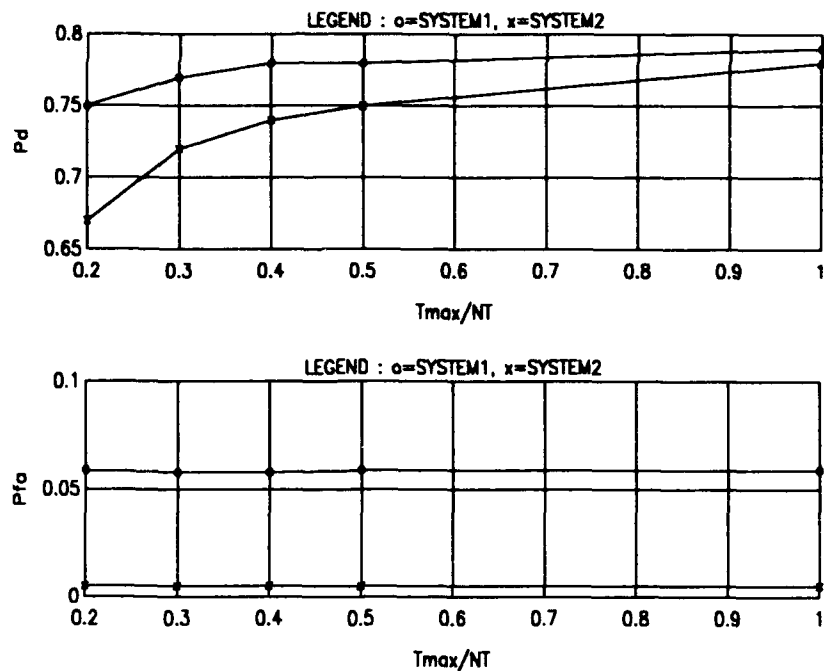**Figure 3.4** Optimal α and β values with respect to the Thychebyceff's Inequality.
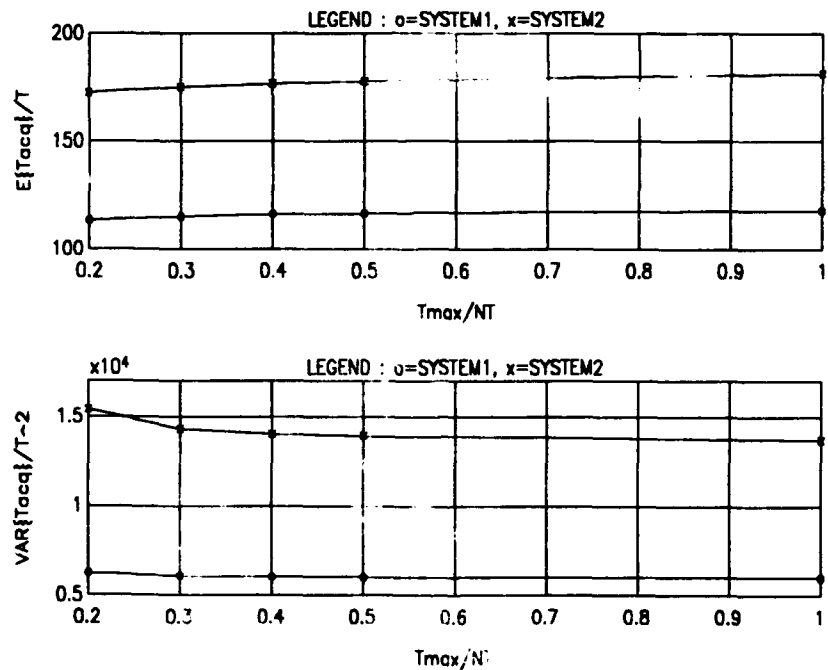

Figure 3.5 Optimal performance parameters with respect to the Thychebycheff's Inequality.

36

values decrease, but the change in either of these is not so drastical. This is because these parameters are essentially determined by α^*, which remains constant for the whole range.

Had the value of T_{max} been specified by the system designer, we could use that value in our equations for further discussion. Since we do not have a predetermined value, we will narrow our focus to the minimum σ^2_{TACQ} choices for the remainder of this thesis. We will also present the results for minimum μ_{TACQ} choices where appropriate.

b. The Effects of The Penalty Time

The *penalty time* for our system was defined as the amount of bit intervals elapsed for returning from the *FA* state. It is essentially determined by the external *tracking* circuit as a measure of the quality of the scheme. Recall from Chapter II that the penalty time was expressed as cNT_c, where c denoted the number of data bits, N was the sequence length and T_c was the chip period. Using the flow graph technique and selecting the minimum variance choices we have calculated α^*, β^*, and normalized μ^*_{TACQ} and σ^{2*}_{TACQ} while the c parameter is varied from 1 bit period to 1000 bit periods. Figure 3.6 depicts the results for the system of example 1 from Table 3.1.

Increased penalty time prolonged the average acquisition time and increased the variance as naturally expected. As far as the design parameters are concerned, we see that β^* is not affected, since the penalty only occurs at H_0 states. The α^* is not affected very much either, if the variation of the penalty time remains in close vicinity of its design value. The system, however, requires a much lower design α to compensate, for an excessively large penalty time.

37
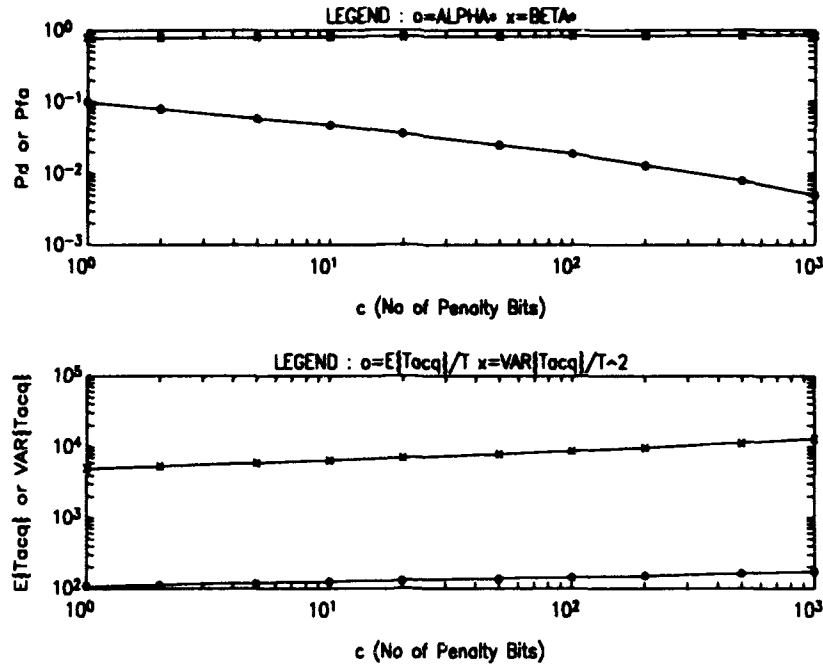
Figure 3.6 The effects of penalty time on the design parameters.

Using the design values shown in Figure 3.6, we can now examine the system behavior for the cases where actual penalty time differs than specified in the design. We have considered three design values of the penalty time, where c = 5, 50 and 500 bit periods. The system is constructed using the corresponding α and β for each case from Figure (3.6). The actual penalty time is again varied from 1 to 1000 bit periods. The variation of σ^2_{TACQ} with the changing penalty time is given in Figure 3.7. We saw that if the system spent more time than specified in the design to recover from a false alarm state, this would degrade the system performance. This degradation would effect the system more severely, especially when the specified penalty time is small and actual penalty takes considerably longer time. Consider our example, the system designed using c = 5, results in a variance value 1.95 times higher than the system designed using c =

38

50 when the actual penalty time (c_A) is 50 bit periods, whereas the second system has only 1.2 times greater variance value than the first system at $c_A = 5$ and the degradation gets worse as c_A increases. Although, we have shown here some extreme cases, this behavior of the system is still valid for a smaller scale of the change in the penalty time. Therefore, we can say that if some uncertainty exists about the penalty time, it is safer to design the system using highest possible c value.

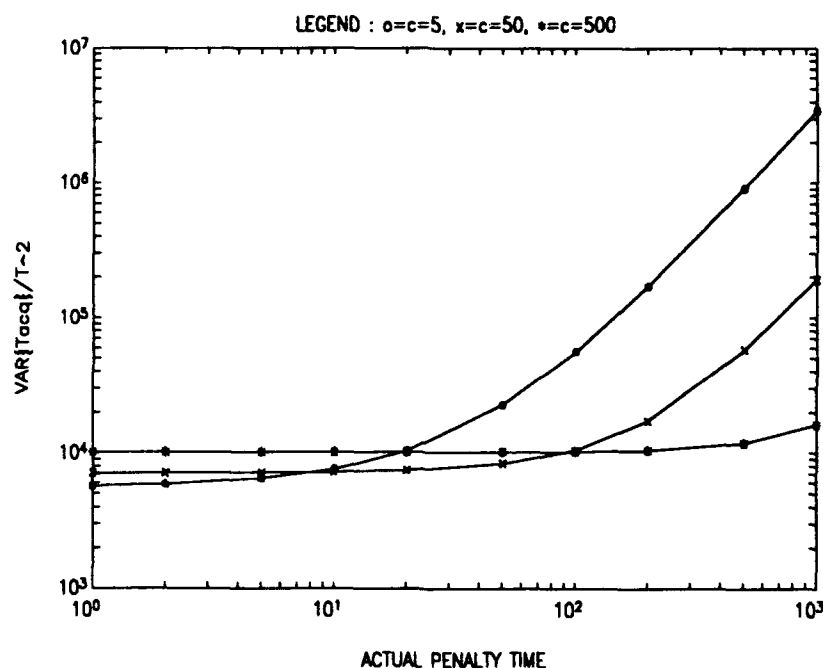

LEGEND : o=c=5, x=c=50, •=c=500

Figure 3.7 The variation of $\sigma^2{}_{TACQ}$ with the actual penalty time.

c. The Channel Mismatch Problem

We will now examine a more serious and practically important design problem of the acquisition system. Recall from equation (2.11) that the chip signal to noise ratio (SNR) of the incoming signal had to be specified prior to designing the

39

system. In practice, for the receiver's site there is no way of knowing the exact SNR other than obtaining this value by field measurements and this effective SNR value may be different than specifications for a variety of reasons, i.e., the receiver's location, channel medium, fading.

Using equation (2.11) we can show that the bit signal to noise ratio, denoted by SNR_b can be expressed as $SNR_b = (A_0^2 T / 2N_0) = N\, SNR$. Here N is the sequence length and T is the bit period. So far, for our examples we fixed the per-chip SNR as -10 dB, which corresponds to an SNR_b of 20 dB. Table 3.2 depicts various design SNR values and the resulting μ^*_{TACQ} and σ^{2*}_{TACQ} using minimum variance choices for the system of example 1.

We will define the term *"channel mismatch"* as the response of the receiver to the incoming signals that have different SNR than specified in the initial design. Naturally, under occurrence of such an event some performance degradation should be expected. This degradation will happen for the stronger signals, as well as for the weaker signals, because lower design SNR will yield a lower threshold which can result an increase in the number of false alarms for stronger signals.

Using the flow graph technique we present the variations of resulting mean and the variance of the acquisition time with respect to the *effective SNR* of the incoming signal. The system of example 1 is used for three separate *design SNR* values (-13, -10 and -3 dB) from Table 3.2. The *effective SNR* is changed from -20 dB to 0 dB for all three cases and the plots for μ_{TACQ} and σ^2_{TACQ} are given in Figures 3.8 and 3.9 respectively.

TABLE 3.2 The system values for various design *SNR* for the acquisition system.

SNR (dB)	SNR$_b$(dB)	$\alpha^{\bullet}$	$\beta^{\bullet}$	$\mu^{\bullet}_{\mathrm{TACQ}}$	$\sigma^{2\bullet}_{\mathrm{TACQ}}$
-20.0	10.0	0.12	0.75	927.0272	4.2269e5
-13.0	17.0	0.07	0.79	219.1580	2.0658e4
-10.0	20.0	0.06	0.80	119.0972	6.0020e3
- 3.0	27.0	0.04	0.81	39.9832	4.4971e2
0.0	30.0	0.03	0.81	20.4277	1.6984e2

For all of the three cases, we can say that the degradation caused by the *stronger* signals are much less than by weaker signals. For example; for the case of *design SNR* = -10 dB, a 10 dB increase in the effective *SNR* increases μ_{TACQ} by a factor of 3, whereas a -10 dB decrease increase the same parameter by a factor of 100. Also, one can observe that in the close vicinity of the *design SNR* slightly stronger signals yield a better performance.

Therefore, if the system designer has some uncertainty about what the received *SNR* would be, it is better to design the system using the lowest possible *SNR* to counterbalance the channel mismatch problem.

3. The Coincidence Detector Parameters

In Chapter II we have proposed a majority logic verification scheme for our system to counter balance the effects of costly false alarms. Briefly, the system will enforce *A* or less additional tests in case of an H_1 decision to verify the correctness. If *B* of the additional tests are in favor of the original decision the system decides H_1. We also assumed that a counter is available and the test can be early terminatable once *B*
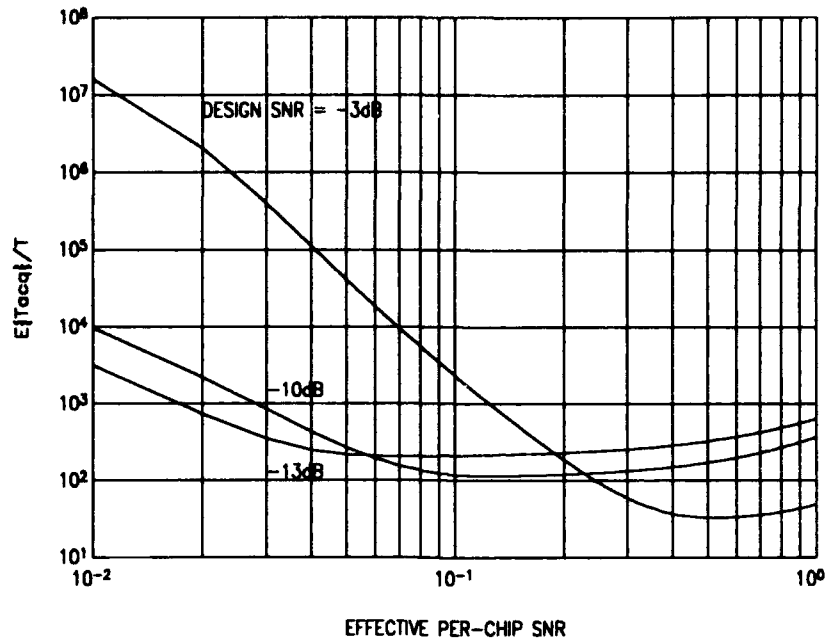
41

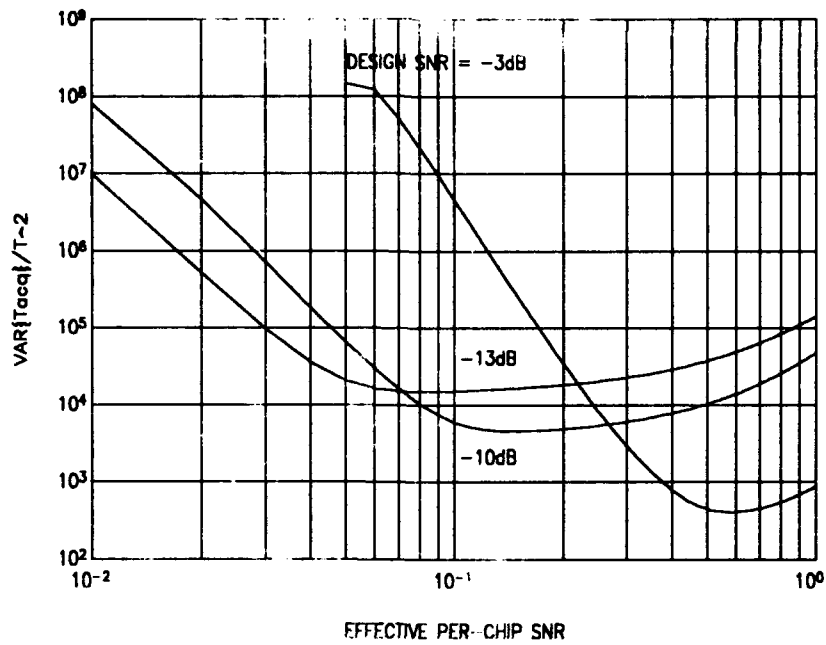**Figure 3.8** The variation of μ_{TACQ} with the effective per-chip SNR.

Figure 3.9 The variation of σ^2_{TACQ} with the effective per-chip SNR.

42

favorable tests are accumulated or there is no chance that B favorable tests can be obtainable. In this section we will investigate what good choices of the parameters A and B should be, with the help of the flow graph technique.

We have calculated minimum σ^2_{TACQ} and corresponding α^* and β^* values for several coincidence detector (CD) parameter pairs (A,B) for the system of example 1, both for with and without early termination feature. We present the results in Figure 3.10 graphically.

The best case for the early terminatable coincidence detector (ETCD) occurs for the (A,B) pair (5,3) resulting a minimum variance of 5715.8 T^2 with $\alpha^* = .09$ and $\beta^* = .82$ and the corresponding $\mu_{\text{TACQ}} = 117.07$ T. This minimum variance value is the overall best case we have achieved for the system with $SNR = -10$ dB so far. For the non-early terminatable coincidence detector (NETCD) we obtain the minimum $\sigma^2_{\text{TACQ}} = 6486.4$ at (4,2) with $\alpha^* = 0.056$ and $\beta^* = 0.8$, and the corresponding $\mu_{\text{TACQ}} = 123.94$ T.

We can remark that choices of optimal design parameters does not change very much regarding to the coincidence detection scheme. One can also see that for this minimum variance cases the improvement achieved using an early terminatable coincidence detector is approximately 5 % in the mean 12 % in the variance.

Although we show only a portion of the results, we have also studied the cases of $7 \leq A \leq 9$ and the results are omitted, because none beats the minimum choices presented above. In fact, it is logical to conclude that choosing A too large is unacceptable for both schemes, although using a ETCD increases the range a little.

43

VARIANCE [Tacq] / T^2 α AND β

13000
12000
11000
10000
9000
8000
7000
6000
5000
4000

1
0.9
0.8
0.7
0.6
0.5
0.4
0.3
0.2
0.1
0

(A,B)

(1,1) (2,1) (2,2) (3,1) (3,2) (3,3) (4,1) (4,2) (4,3) (5,1) (5,2) (5,3) (5,4) (6,1) (6,2) (6,3) (6,4) (6,5)

Legend
EARLY TERM (ET)
NO EARLY TERM (NET)
(ET) β*
(ET) α*
(NET) β*
(NET) α*
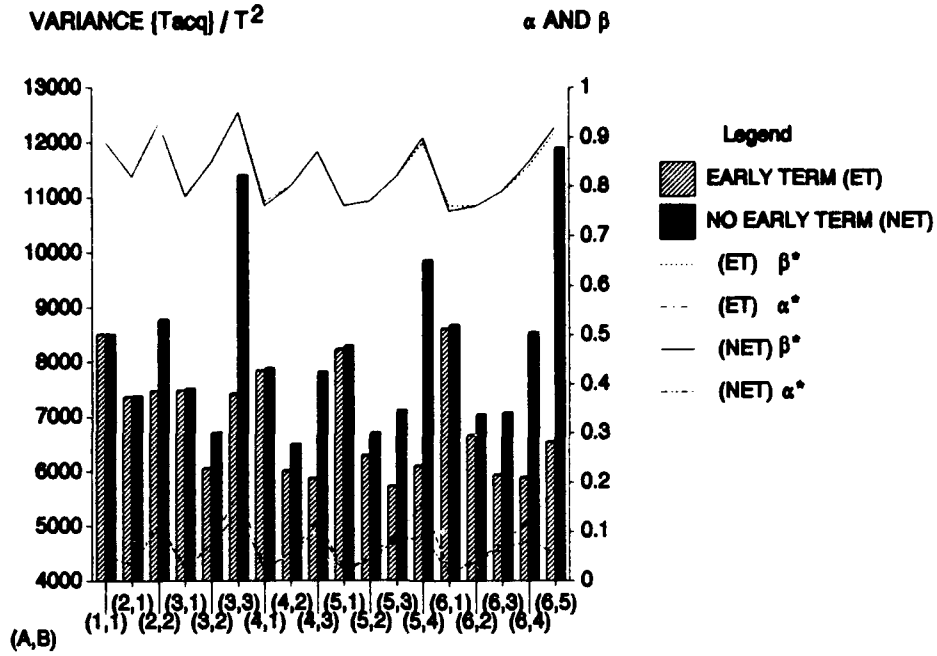
Figure 3.10 Minimum σ^2_{TACQ} and α^*, β^* versus various coincidence detector parameters.

From Figure 3.10, we can conjecture that once A is fixed the optimal choice of B is around $\lfloor A/2 \rfloor$. We can qualitatively verify this hypothesis by the following argument. Recall from Chapter II that the coincidence detection or false alarm probability is given by the cumulative binomial distribution of the form

$$P_c = P(B \le X \le A) = \sum_{j=B}^{A} \binom{A}{j} p^j (1-p)^{A-j} \qquad (3.11)$$

where the random variable X represents the event that an acquisition decision (either genuine or falsely) is made and p denotes the *detection* or *false alarm* probability for a single test. This distribution has the mean pA and the variance $p(1-p)A$. The value of P_c equals to unity for $B=0$ regardless of the value of p. Considering (3.11) one can see that

for a fixed A, a small p, i.e., a typical false alarm probability, results in a small mean and variance, therefore, P_c decreases rapidly with the increasing B. On the other hand a large p, i.e., a typical detection probability, results a large mean (close to A) and variance, therefore, rapid deteoration in P_c occurs for large values of B. The system does not know in advance whether an initial H_1 decision will result in FA or ACQ state, therefore, uses the same CD parameters for both cases. We want a large B to pull down the P_{cfa} as low as possible, while a small B will make P_{cd} as high as possible. Therefore an optimum B exists in the interval [0 A]. Considering all the other factors effecting the resulting μ_{TACQ} and σ^2_{TACQ}, it happens to be around $\lfloor A/2 \rfloor$.

4.   Simulation Results

Our study on the *FSS* serial search acquisition scheme was based on approximations and analytical formulations. In this section we present simulation results for some particular cases to verify the validity of our assumptions and analyses.

We have used an m-sequence of length 1023 with the primitive generator polynomial $1 + x^2 + x^5 + x^6 + x^{10}$. The value of γ used for the design is 0.5. The update fraction, Δ, of the local m-sequence is set to be 1/2, half the chip period. The initial state *a priori* distribution is assumed to be uniform. The early terminatable coincidence detector parameters are taken as $A=4$ and $B=2$.

The simulations are performed using the three different per-chip design *SNR* values from Table 3.2 (-13dB,-10dB and -3dB) for 1000 runs. The sample and theoretical values of μ_{TACQ} and σ^2_{TACQ} are given in Table 3.3.

45

TABLE 3.3 The simulation results for various per-chip *SNR* .

SNR (dB)	Sample μ_{TACQ}	Theoretical μ_{TACQ}	Sample σ^2_{TACQ}	Theoretical σ^2_{TACQ}
-13.0	217.10	219.16	19212.0	20658.0
-10.0	116.33	119.09	5494.6	6002.0
-3.0	36.82	39.98	574.7	449.7

Finally, we present the histogram for the case of per-chip *SNR* = -10 dB to give an idea about the shape of the probability distribution function $f_{Tacq}(t_{acq})$ in Figure 3.11.
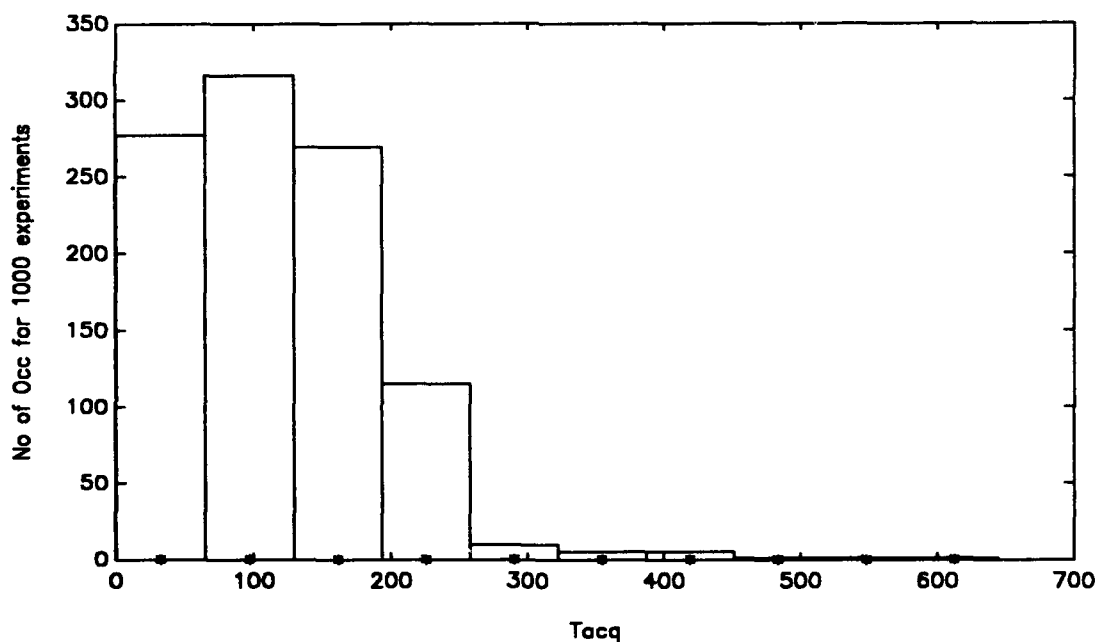

Figure 3.11 Histogram for the simulation of the FSS scheme.

C. SEQUENTIAL AND TRUNCATED SEQUENTIAL PROBABILITY RATIO TESTS

The sequential probability ratio test (SPRT) for the acquisition scheme of Chapter II, is obtained by testing the likelihood ratio of (2.8) against two thresholds for $n = 1,2,3...$ until one of the thresholds is exceeded. The length of the integration increases by one chip each time n increases by one. The resolvement between the hypotheses H_0 and H_1 is achieved by checking which threshold value is reached first. The test can be written as

$$SPRT: \quad \Lambda_n(y_n) \begin{cases} \geq A & say\ H_1 \\ \leq B & say\ H_0 \\ otherwise,\ continue\ to\ next\ n \end{cases} \tag{3.12}$$

Note that Y_n and Y_{n+1} are not independent and the likelihood ratio $\Lambda_n(y_n)$ can not be written as the sum of independent random variables. However, Type I error (false alarm probability) and Type II error (miss probability) can still be related through Wald's inequalities[Ref. 14],

$$A \leq \frac{1-\beta_m}{\alpha} \qquad and \qquad B \geq \frac{\beta_m}{1-\alpha} \tag{3.13}$$

where α and β_m ($=1-\beta$) are the resulting false-alarm and miss probabilities, respectively. If the excess over the boundary is small when the test terminates, which is the case when the average test length is large, the inequalities in (3.13) can be approximated by equalities. Since $1-\beta_m < 1$ and $1-\alpha < 1$, we can write

47

$$\alpha < \frac{1}{A} \qquad and \qquad \beta_m < B \qquad\qquad (3.14)$$

which is useful when strict upper bounds on the errors are desired. These bounds are tight when the errors and the signal-to-noise ratio are small.

Using the monotonicity of the likelihood ratio, the test in (3.12) can be written in a more practical form for real time implementations, as

$$y_n \begin{cases} \geq A(n) = \Lambda_M^{-1}(A) & say\ H_1 \\ \leq B(n) = \Lambda_M^{-1}(B) & say\ H_0 \\ otherwise,\ continue\ to\ next\ n \end{cases} \qquad (3.15)$$

where the thresholds can be precomputed as functions of n.

The SPRT has been shown to be optimum, in the sense of minimizing the average test length under H_0 and H_1, only when the samples are i.i.d.[Ref. 6]. But for our situation the samples are non-i.i.d. and no optimality has been established. However, we expect that the performance is still good and much better than the FSS test.

The SPRT test has a drawback that for certain PN sequence phase disparities, it may take an excessively long time to resolve between the two hypotheses. Such an incident is especially likely when the initial phase difference between the two PN sequences fall in the state between H_0 and H_1 as shown in (2.7). To avoid a lengthy test, a truncated SPRT (TSPRT) test was proposed in [Ref 7], which imposed an upper bound on the test length. The test is described by

48

$$TSPRT: \quad if\ n \leq \hat{n}, \quad \Lambda_n(y_n) \begin{cases} \geq \hat{A} & say\ H_1 \\ \leq \hat{B} & say\ H_0 \\ otherwise, & continue \end{cases} \quad (3.16)$$

$$if\ n = \hat{n}, \quad \Lambda_n(y_n) = \Lambda_{\hat{n}}(y_{\hat{n}}) \begin{cases} \geq \hat{\tau} & say\ H_1 \\ < \hat{\tau} & say\ H_0 \end{cases}$$

The test is truncated at $n = \hat{n}$ and converted to a FSS test if it has not terminated before. Again using the monotonicity of the likelihood ratio function the test can be written as

$$TSPRT: \quad \begin{aligned} if\ n \leq \hat{n}, \quad y_n & \begin{cases} \geq \hat{A}(n) = \Lambda_n^{-1}(\hat{A}) & say\ H_1 \\ \leq \hat{B}(n) = \Lambda_n^{-1}(\hat{B}) & say\ H_0 \\ otherwise, & continue \end{cases} \\ if\ n = \hat{n}, \quad y_{\hat{n}} & \begin{cases} \geq \Lambda_{\hat{n}}^{-1}(\hat{\tau}) & say\ H_1 \\ < \Lambda_{\hat{n}}^{-1}(\hat{\tau}) & say\ H_0 \end{cases} \end{aligned} \quad (3.17)$$

1. **Design Of Decision Processors**

The thresholds A and B for the SPRT test can be calculated using

$$A = \frac{1}{\alpha} \quad and \quad B = \beta_m. \quad (3.18)$$

From (3.15), one can see that the resulting false alarm and miss probabilities are $P_{fa} \leq 1/A = \alpha$ and $P_{miss} \leq B = \beta_m$.

To devise thresholds for the TSPRT, we will split the test into two parts. Consider that the test consists of a SPRT with thresholds $\hat{A}$, $\hat{B}$ and errors α_{sprt}, β_{sprt} and

49

a FSS test with sample size $\hat{n}$, threshold $\hat{\tau}$ and errors α_{fss}, β_{fss}. It was shown in [Ref. 7]

that the errors of the TSPRT (3.17) were bounded by

$$
\begin{aligned}
\alpha_{tsprt} &\leq \alpha_{sprt} + \alpha_{fss}, \\
\beta_{tsprt} &\leq \beta_{sprt} + \beta_{fss}.
\end{aligned}
\tag{3.19}
$$

Therefore, to obtain $\alpha_{tsprt} \leq \alpha$ and $\beta_{tsprt} \leq \beta_m$, we can split these errors into

the sums of the errors due to the SPRT and the errors due to the FSS test. Specifically,

we let

$$
\begin{aligned}
\alpha &= \alpha_{sprt} + \alpha_{fss} = p_0\alpha + (1-p_0)\alpha, \\
\beta &= \beta_{sprt} + \beta_{fss} = p_1\beta_m + (1-p_1)\beta_m
\end{aligned}
\tag{3.20}
$$

where p_0 and p_1 are constants in [0,1]. By setting $\alpha_{sprt} = p_0\alpha$ and $\beta_{sprt} = p_1\beta_m$, we can

design the thresholds $\hat{A}$ and $\hat{B}$ according to (3.18). Similarly letting $\alpha_{fss} = (1-p_0)\alpha$ and

$\beta_{fss} = (1-p_1)\beta_m$, $\hat{n}$ and $\hat{\tau}$ can be obtained using (3.5). Note that if $p_0 = p_1 = 0$ the TSPRT

becomes an FSS test, while setting both parameters to unity converts the test a pure

SPRT. Hence for values in between, the TSPRT can be considered a mixture of SPRT

and FSS test.

2. Mean and Variance Analysis of The TSPRT Scheme

It was shown in [Ref. 7] that a properly designed TSPRT was superior to the

FSS test in the average sample number (ASN) for a single search state. It was also found

that TSPRT and SPRT performed very close. For the remainder of this chapter we will

focus our attention to the TSPRT and make an overall acquisition system analysis using

the flow-graph technique.

50

The system model depicted in Section B of Chapter II remains the same, only the decision processor is replaced with a TSPRT scheme. However, the time delays associated with each state are now random variables instead of constants as were in the FSS scheme. Therefore we will use the statistical averages, namely $E\{t_i\}$, $E\{t_i^2\}$, $E\{t_i'\}$ and $E\{t_i'^2\}$ in place of the constant time delays of the FSS test, to obtain μ_{TACQ} and σ^2_{TACQ} for this system. Recalling the equations from Chapter II and using the same notation and symmetry conditions, the required parameters for the analysis are

$$
\begin{aligned}
E(t_{d1}) &= ASN_{-1.5}.T_c = ASN_{1.5}.T_c,\\
E(t_{d2}) &= ASN_{-0.5}.T_c = ASN_{0.5}.T_c,\\
E(t_{fa}) &= ASN_{-2.0}.T_c = ASN_{2.0}.T_c,\\
E(t_{d1}^2) &= (VSN_{1.5} + [ASN_{1.5}]^2).T_c^2,\\
E(t_{d2}^2) &= (VSN_{0.5} + [ASN_{0.5}]^2).T_c^2,\\
E(t_{fa}^2) &= (VSN_{2.0} + [ASN_{2.0}]^2).T_c^2
\end{aligned}
\tag{3.21}
$$

where ASN denotes the "average sample number", while VSN stands for "variance of the sample number". The delays associated with the coincidence detector are

$$
\begin{aligned}
E(t_i') &= c_i.E(t_i),\\
E(t_i'^2) &= c_i^2.E(t_i^2)
\end{aligned}
\tag{3.22}
$$

where c_i is a known constant(see equation (2.21)). The values of ASN, VSN and all the detection and false alarm probabilities can be found using simulation techniques described in [Ref. 7].

51

a. Optimal Choices of Design Parameters

For the TSPRT test we followed a similar approach to that of the FSS scheme. However in this case we do not have closed form expressions, therefore, we have to depend solely on the simulation results.

Specifying the desired false-alarm and detection probabilities suffices to design a TSPRT processor as described above. We will be looking for the two design parameters α^* and β^* which minimize the variance of the acquisition time.

We again consider the acquisition scheme depicted in example 1 of Section B. The decision processor is replaced with a TSPRT scheme and a m-sequence with period $N=1023$ is used as the PN sequence. The mixture rates are taken as $p_0 = p_1 = 0.5$. The simulations are executed for various α, β pairs, where $\alpha \in \{0.001, 0.01, 0.05, 0.1, 0.15, 0.2\}$ and $\beta \in \{0.5, 0.6, 0.7, 0.8, 0.9\}$. We have also considered several coincidence detector parameters A and $B \in [0,8]$.

For all the cases, all of the actual P_d values came out to be slightly greater than β's, while all the actual P_{fa} values were slightly less than α's, which indicated that the system setup and approximations worked well.

Among all the cases investigated, the variance is minimized by the pair ($\alpha^*=0.05$, $\beta^*=0.6$) with the coincidence detector parameters $A=5$ and $B=2$. All the relevant parameters associated with these design parameters are given in Table 3.4.

The notable improvement of the TSPRT over the FSS scheme can be clearly seen from these results. Recalling the best case of FSS scheme, the variance of the acquisition time is decreased from 5715.8 T^2 to 2461.4 T^2, (approximately 57 %

52

TABLE 3.4 The results of the TSPRT scheme.

A = 5 B = 2 SNR = -10 dB $\gamma = \Delta = 0.5$ $\alpha^* = 0.05$ $\beta^* = 0.6$	$E(t_{d1}) = 73.4800\ T_c$	$E(t_{d1}^2) = 6121.0\ T_c^2$
	$E(t_{d2}) = 63.1390\ T_c$	$E(t_{d2}^2) = 4751.0\ T_c^2$
$\mu_{TACQ} = 72.1909\ T$ $\sigma^2_{TACQ} = 2461.4\ T^2$	$E(t_{fa}) = 56.1900\ T_c$	$E(t_{fa}^2) = 3720.2\ T_c^2$
$P_{d1} = 0.7660$	$E(t_{d1}') = 190.40\ T_c$	$E(t_{d1}'^2) = 41096\ T_c^2$
$P_{d2} = 0.0840$	$E(t_{d2}') = 267.15\ T_c$	$E(t_{d2}'^2) = 85057\ T_c^2$
$P_{fa} = 0.0288$	$E(t_{fa}') = 230.51\ T_c$	$E(t_{fa}'^2) = 62609\ T_c^2$

decrease), while the mean acquisition time is also improved by approximately 38.3 % for the same design parameters. We remark that this improvement is a result of decreasing the average sample size per state, while keeping the actual probability of detection and probability of false alarm within reasonable values. Note that the actual P_d is greater than β and the actual P_{fa} is less than α, which is usually the case, because the system is designed on a nominal worst case basis.

The minimum μ_{TACQ} for the design example is 70.1626 T and the corresponding $\sigma^2_{TACQ} = 2814.3\ T^2$. These values occur for the (α,β) pair (0.05,0.5). As we can see that we still have a different set of parameters for minimum average acquisition time choices as we had for the FSS scheme. But the values are somewhat closer for the TSPRT so that our argument for selection of the design parameters using the *Thebycheff's Inequauty* holds even more confidently for the TSPRT scheme.

53

As one can see, we again have a small α value and a moderate β value to minimize either the mean or the variance of the acquisition time. The ASN and VSN increases with the increasing β and decreasing α (see Figure 3.12). Increasing β excessively affects ASN and VSN, especially under H_0 hypothesis. Since a very large portion of the total states fall under H_0, this results a large mean and variance. Therefore, the system is optimized on H_0 by keeping α low to reduce the effects of false alarms, and keeping β reasonably moderate, not to increase the ASN and VSN excessively.

To certify the improvement achieved using a TSPRT scheme over the FSS scheme, the simulations are repeated for two other per-chip design SNR values (-13
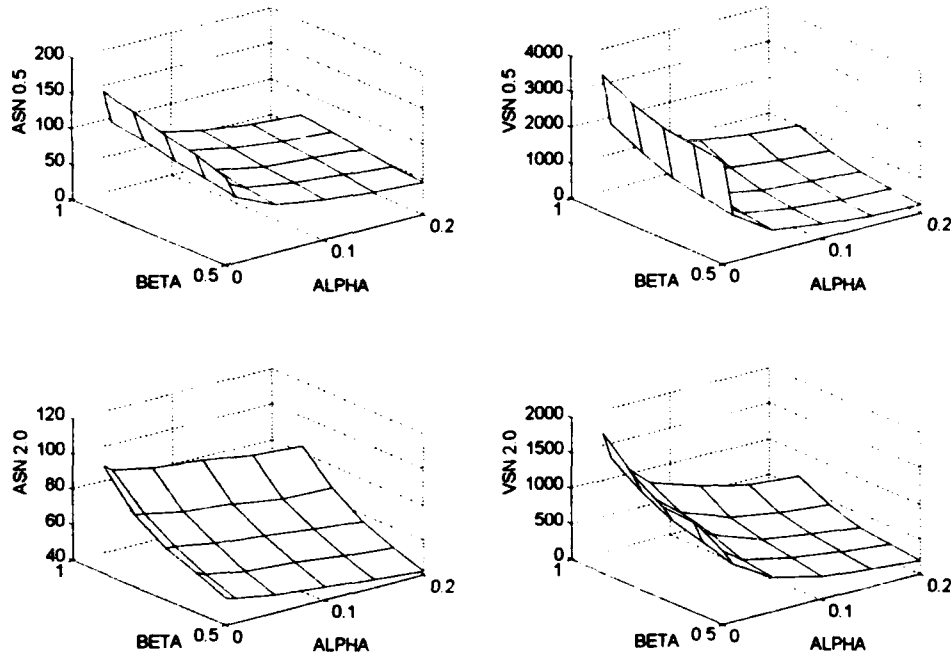
Figure 3.12 The variation of ASN and VSN with various α and β.

dB and -3 dB) with all the other parameters remained fixed. Figures 3.13 and 3.14 compare the mean and the variance of the acquisition time with the results given in Table 3.2 for the FSS scheme.
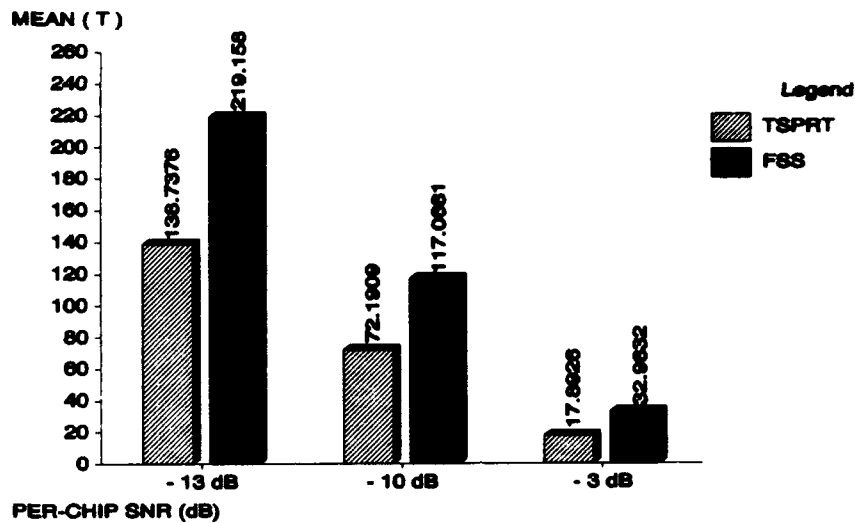

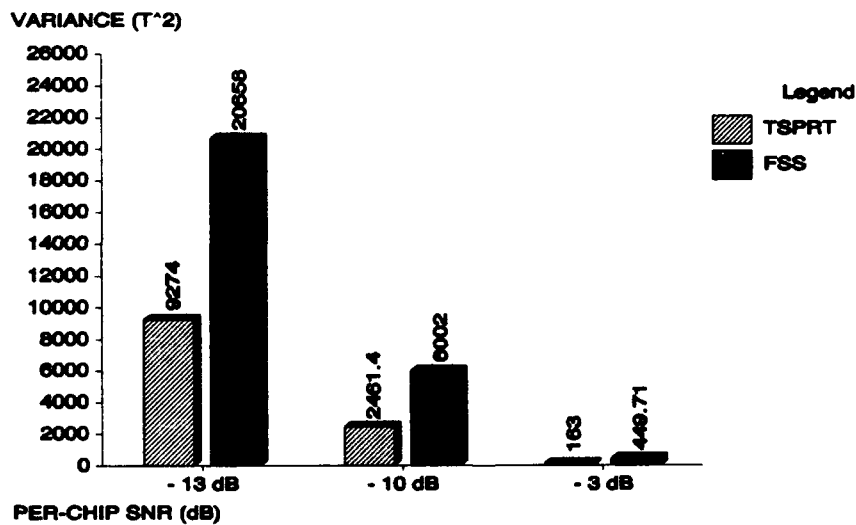**Figure 3.13** The resulting μ_{TACQ} for various design SNR values.

Figure 3.14 The resulting σ^2_{TACQ} for various design SNR values.

b. The Channel Mismatch Problem

We examined the *channel mismatch* for the TSPRT scheme in a similar fashion that we did for the FSS scheme. The system given in Table 3.4 is designed using the three separate per-chip SNR values (-13, -10 and -3 dB) from Figures 3.13 and 3.14. The *effective SNR* of the incoming signal is varied from -20 dB and 0 dB for all the three cases and the plots for μ_{TACQ} and σ^2_{TACQ} are given in Figures 3.15 and 3.16 respectively.

We see a very similar picture to that of the FSS scheme. The degradation caused by weaker signals are far greater than the stronger signals and this degradation is more severe for higher design SNR (SNR_d). As a numerical example, for $SNR_d = 0.1$ the mean value is increased by a factor of 291 by a decrease of -10 dB in effective SNR, while a 10 dB increase, elevates the same parameter by only a factor of 3.44. For all of the three cases, slightly stronger signals in vicinity of the SNR_d actually yield a slightly better performance.

As a final observation, we can see that the aforementioned degradation for the weaker signals seem to be slightly more severe for the TSPRT scheme than the FSS scheme, i.e., the curves are steeper. This behavior is consistent, since the TSPRT scheme is along the optimality boundary, therefore more sensitive to the external effects.

From all this discussion, we can once again conclude that if the system designer has some uncertainty about what the received SNR would be, it is better to design the system using lowest possible SNR_d to counter balance the channel mismatch problem. More will be said about the degradation in effective SNR in the next chapter when we examine the effects of fading on the performance.
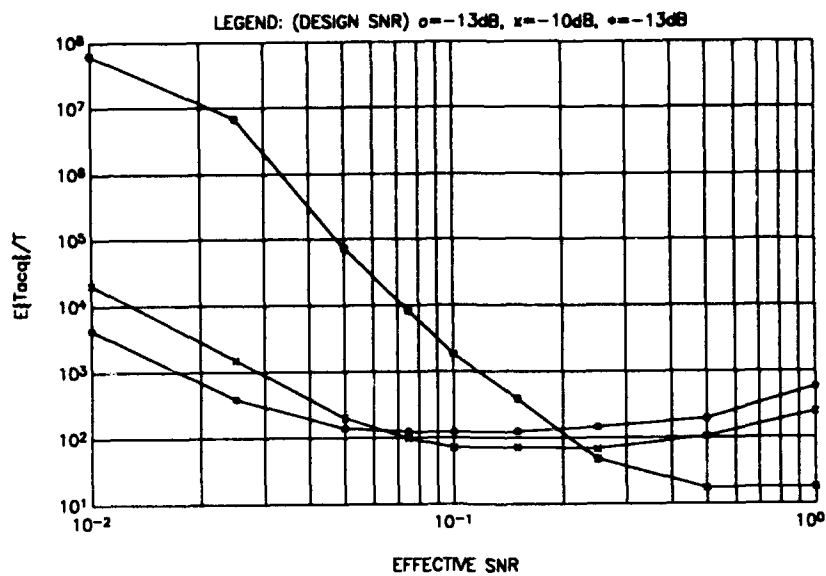
56

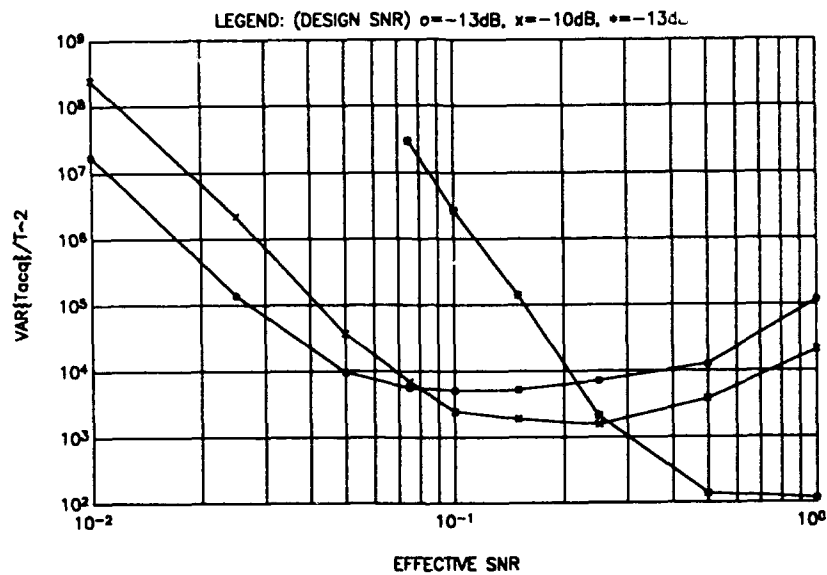**Figure 3.15** The variation of μ_{TACQ} with the effective per-chip SNR for the TSPRT.

Figure 3.16 The variation of σ^2_{TACQ} with the effective per-chip SNR for the TSPRT.

57

IV. PERFORMANCE IN THE FADING MULTIPATH CHANNEL

A. INTRODUCTION

The previous chapters have described the design and performance of the acquisition

systems operating over the classical AWGN channel.

In this chapter we consider the problem of the receiver performance for more

complex channels, namely, channels having randomly time-variant impulse responses.

This characterization serves as a model for signal transmission over many radio channels

such as shortwave ionospheric radio communication in the HF frequency band,

tropospheric scatter (beyond-the-horizon) radio communications in the UHF and SHF

bands, and ionospheric forward scatter in the VHF frequency band [Ref. 15]. The time-

variant impulse responses of these channels are a consequence of the constantly changing

physical characteristics of the media. As an example, the ions in the ionospheric layers

that reflects the signals are always in motion which appears to be random to the user f

the channel.

Although fading arises from variety of reasons, fading phenomena can often be

modeled as causing multipath distortion. That is, many fading conditions can be modeled

as causing several alternate transmission routes to arise between the transmitter and the

receiver. Since this multipath is a result of the time varying characteristic of the channel,

the nature of the multipath varies with time. That is, in addition to the transmission path

which the system designer considered, additional unplanned transmission path varying

with time and appearing as random to the user of the channel are excited. The signals arriving at the receiver through different paths interfere either constructively or destructively to result in signal fading. Since this variations appear to be random, fading is best described using statistical terms.

Fading is a widely studied area of the communication theory and more detailed explanation about the topic can be found in existing literature.

Our intent for this chapter is to examine the effects of fading on our acquisition receiver performance. Effect of fading on the very same system was previously studied in [Ref. 10] for a single search state cell basis to examine the variation of the average test length, the detection and the false alarm probabilities for the TSPRT scheme. We will extend this study to the overall system basis using the flow-graph technique.

B.   MATHEMATICAL MODEL

The fading multipath channel under consideration is characterized as *flat* and *slow* fading channel. Flat in this context means that fading affects all frequency components present in the transmitted signal in exactly the same manner as opposed to *bandwidth-selective* channels. The received signal in such a case can be regarded as multiplied by a random variable which accounts for the fading. The other characterization, slow means that the channel variations (which give rise to the signal power fluctuations) are slower than the lowest frequency component in the signal. Therefore, the received signal can again be regarded as multiplied by a random variable, rather than by a fluctuating time function which would be the case for fast fading channels.

In the multipath approximation, the power in the stronger signal path for which the system is intended to be designed, is called the *direct component*, while all the total power in the remaining weaker paths is termed as the *diffuse component*.

It has been shown in [Ref. 10] that for the assumed flat, slowly varying fading channel, the received signal is effectively multiplied by a random coefficient ψ which has a Ricean probability density function, given by

$$f_{\psi}(\psi) = 2\psi(1+r)e^{-r-\psi^2(1+r)}I_0(2\psi\sqrt{r(1+r)}), \quad \psi > 0 \qquad (4.1)$$

where r the ratio of the power in the direct component (s^2) and the power in the diffused component ($2\sigma^2$), with the constraint that $s^2 + 2\sigma^2 = 1$. The parameters s^2, σ^2 and hence r are dependent on the nature of the channel. Note that for $r = \infty$ (or $s^2=1$ and $\sigma^2=0$), it corresponds to no fading. Also when $r=0$ (or $s^2=0$ and $\sigma^2=0.5$) we have Rayleigh fading, of which the pdf is given by

$$f_{\psi}(\psi) = 2\psi e^{-\psi^2}, \quad \psi > 0. \qquad (4.2)$$

C. TEST STATISTICS DENSITY FUNCTION

Recall from Chapter II that the receiver's (Figure 2.1) test statistics is given by equation (2.6). Assuming a slowly varying, flat fading multipath channel the resulting test statistics can be found as follows. The received signal through the fading channel is now given as

$$r(t) = A_0 \psi a(t + i\Delta T_c)\cos(\omega_0 t + \theta) + n(t) \qquad (4.3)$$

where ψ is the fading random variable with the pdf of (4.1) or (4.2). Note that since we have assumed slowly varying fading channel, ψ does not change very much within one data bit interval, therefore can be assumed constant during the test length. Referring to the receiver structure the inphase and the quadrature components depicted in equation (2.2) now become

$$X_{i,n} = \frac{A_0}{2}\psi T_c S_n \cos\theta + N_{i,n},$$
$$X_{q,n} = \frac{A_0}{2}\psi T_c S_n \sin\theta + N_{q,n} \qquad (4.4)$$

where $N_{i,n}$ and $N_{q,n}$ are still defined by equation (2.3). As before, the test statistic for determining the alignment is

$$Y_n = X_{i,n}^2 + X_{q,n}^2. \qquad (4.5)$$

The conditional probability density function of y_n conditioned on ψ, is non-central Chi-squared, and given by

$$f_{Y_n|\psi}(y_n|\psi) = \frac{1}{2\sigma_n^2}e^{-(y_n + \lambda_n\psi^2)/2\sigma_n^2}I_0\left(\frac{\sqrt{\lambda_n\psi^2 y_n}}{\sigma_n^2}\right), \qquad y_n > 0 \qquad (4.6)$$

where $\lambda_n = (A_0^2/4)T_c^2 S_n^2$ and $\sigma_n^2 = nT_c N_0/4$.

It follows from the above equation that to determine the test statistic's density function, the ψ dependance has to be integrated out. Namely, the test statistics density function is

$$f_{Y_n}(y_n) = \int_0^\infty f_{Y_n}(y_n|\psi)\, f_\psi(\psi)\, d\psi. \tag{4.7}$$

In the previous study [Ref. 10] this integral was carried out using the probability density functions of equations (4.1) and (4.6). The resulting pdf of new test statistics under fading conditions is repeated below.

$$f_{Y_n}(y_n) = \frac{1+r}{2\sigma_n^2[(1+r)+\lambda_n/2\sigma_n^2]}\, exp \left[\frac{-[(1+r)(y_n/2\sigma_n^2)+r(\lambda_n/2\sigma_n^2)]}{(1+r)+\lambda_n/2\sigma_n^2} \right]$$
$$\cdot I_0 \left[\frac{2\sqrt{r(1+r)(y_n/2\sigma_n^2)(\lambda_n/2\sigma_n^2)}}{1+r+\lambda_n/2\sigma_n^2} \right] \tag{4.8}$$

This result shows that the probability density function of y_n is still non-central Chi-squared. The density function is still the same form of equation (2.6) but the parameters λ_n and σ_n^2 are replaced by new values,

$$\lambda_n' = \lambda_n \frac{r}{1+r},$$
$$\sigma_n^{2\prime} = \sigma_n^2 \frac{1+r+\lambda_n/2\sigma_n^2}{1+r}. \tag{4.9}$$

D. PERFORMANCE ANALYSIS TECHNIQUES

Since we have the precise description of the receiver's test statistic density function, we might perform our ongoing analysis methods to examine the performance of the FSS and TSPRT schemes under fading conditions. Note that for the FSS scheme we have closed form expressions and we might perform the analysis analytically. But for the TSPRT scheme we have to depend on simulation results.

62

In the previous study [Ref. 10], the performance under fading conditions is examined using a numerical integration technique to integrate out the ψ dependance from the conditional density function. That technique required a number of simulations, specifically 25 simulations for a single case (because the area under pdf is divided up to 25 intervals). In this thesis we will use a different, more direct simulation technique, that is, we will design our receiver in the normal way without the fading and simulate the effects of fading using the pdf in equation (4.8).

It is instructive to examine the specifics of the simulation technique to verify the validity of the results. In the original simulation program the test was based on the likelihood ratio of (2.8), so that for the SPRT part of TSPRT, i.e., $n < \hat{n}$ (see 3.16), the test is conducted by

$$b = \ln(\hat{B}) \quad \begin{matrix} H_0 \\ < \\ > \\ continue \end{matrix} \quad \frac{\lambda_{n,0} - \lambda_{n,1}}{2\sigma_n^2} + \ln \left[\frac{I_0(\sqrt{(y_n/\sigma_n^2)(\lambda_{n,1}/\sigma_n^2)}\ )}{I_0(\sqrt{(y_n/\sigma_n^2)(\lambda_{n,0}/\sigma_n^2)}\ )} \right] \quad \begin{matrix} H_1 \\ > \\ < \\ continue \end{matrix} \quad a = \ln(\hat{A}) \quad \textbf{(4.10)}$$

where $\hat{A}$ and $\hat{B}$ is calculated using (3.18) and (3.20). The test statistics y_n was then normalized by σ_n^2, i.e., a new random variable was introduced, $z_n = y_n/\sigma_n^2$. With this transformation, the test was written as

$$\hat{b}(n) = b + \frac{\lambda_{n,1} - \lambda_{n,0}}{2\sigma_n^2} \begin{array}{c} H_0 \\ < \\ > \\ cont. \end{array} \ln \left[\frac{I_0(\sqrt{z_n(\lambda_{n,1}/\sigma_n^2)})}{I_0(\sqrt{z_n(\lambda_{n,0}/\sigma_n^2)})} \right] \begin{array}{c} H_1 \\ > \\ < \\ cont. \end{array} \hat{a}(n) = a + \frac{\lambda_{n,1} - \lambda_{n,0}}{2\sigma_n^2} \qquad (4.11)$$

where the thresholds were now functions of n, because $(\lambda_{n,i}/\sigma_n^2)$ depend on n (see equations (2.12) and (2.13)). All $(\lambda_{n,i}/\sigma_n^2)$ values in equation (4.11) were calculated using the nominal worst case values of equation (2.13). The probability density function of the new test statistics z_n was given as

$$f_{z_n}(z_n) = \frac{1}{2} e^{-(z_n + \lambda_z)/2} I_0 (\sqrt{\lambda_z z_n}) \qquad (4.12)$$

where $\lambda_z = \lambda_{n,1}/\sigma_n^2$ under H_1 and $= \lambda_{n,0}/\sigma_n^2$ under H_0. The simulation program generates z_n with this statistics, using the actual values $(\lambda_{n,i}/\sigma_n^2)$ given by equations (2.10) and (2.12), then calculates the value of the middle expression in (4.11) and compares the resulting value with the two thresholds $\hat{a}$ (n) and $\hat{b}$ (n) to resolve between the hypotheses.

We have seen that the fading effects the statistics of y_n in the manner depicted in (4.9). Using the transformation $z_n = y_n/\sigma_n^2$ this changes the probability density function of z_n as

$$f_{z_n}(z_n) = \frac{1}{2(\sigma_n'/\sigma_n)^2} e^{-(z_n + \lambda_n'/\sigma_n^2)/2(\sigma_n'/\sigma_n)^2} I_0 (\sqrt{(\lambda_n'/\sigma_n^2)z_n} / (\sigma_n'/\sigma_n)^2) \qquad (4.13)$$

where the new parameters can be written in terms of the older ones as

64

$$\lambda_z' = \frac{\lambda_n'}{\sigma_n^2} = \frac{\lambda_n}{\sigma_n^2} \frac{r}{1+r},$$

$$\left(\frac{\sigma_n'}{\sigma_n}\right)^2 = \frac{1+r+\lambda_n/2\sigma_n^2}{1+r}.$$

(4.14)

Once r is fixed, we can use equations (4.13) and (4.14) to generate the test statistics, therefore, the effects of fading on the TSPRT scheme can be examined for various fading conditions.

The FSS scheme under fading conditions is easier to examine. We simply use the cumulative distribution function of y_n corresponding to (4.8) to calculate the detection and false alarm probabilities. The cumulative distribution function of y_n can be written as

$$F_{Y_n}(y_n) = 1 - Q\left[\sqrt{\frac{r(\lambda_n/\sigma_n^2)}{1 + r + \lambda_n/2\sigma_n^2}}, \sqrt{\frac{(1+r)(y_n/\sigma_n^2)}{1 + r + \lambda_n/2\sigma_n^2}}\right]$$

(4.15)

where the Q function is defined as equation (3.4).

E.   RECEIVER PERFORMANCE WITH FADING

1.   Numerical Results

We now use the flow graph technique to examine the variations of the performance parameters of the acquisition time, μ_{TACQ} and σ^2_{TACQ} for various fading conditions. The analysis for TSPRT and FSS schemes will follow the steps outlined in Chapter III, Subsection C.2. and B.2. respectively. We first present the numerical results for the best case (minimum variance) design examples of Chapter III for SNR = -10

65

dB. The system for TSPRT has the parameters ($\alpha = 0.05$, $\beta = 0.6$, A=5, B=2) and the FSS system has the parameters ($\alpha = 0.09$, $\beta = 0.82$, A=5, B=3). In these figures the fading conditions is varied for $r \in \{0.0, 0.5, 1.0, 2.0, 5.0, 10.0, 20.0, 50.0, 100.0\}$ for both of the systems.

Figures 4.1 and 4.2 show the variation of the μ_{TACQ} and σ^2_{TACQ} for the fading conditions respectively. Referring to these figures, we can say that severe fading, i.e., $r < 5$ cause a considerable performance degradation for both of the schemes. This degradation is unavoidable if additional counter measures were not taken to reduce the effects of fading. But we can still see that TSPRT performs considerably better than FSS scheme even under severe fading conditions. Note also that as r increases both curves asymptotically approach to their non-fading values, which indicates that the system setup and analysis technique works well.
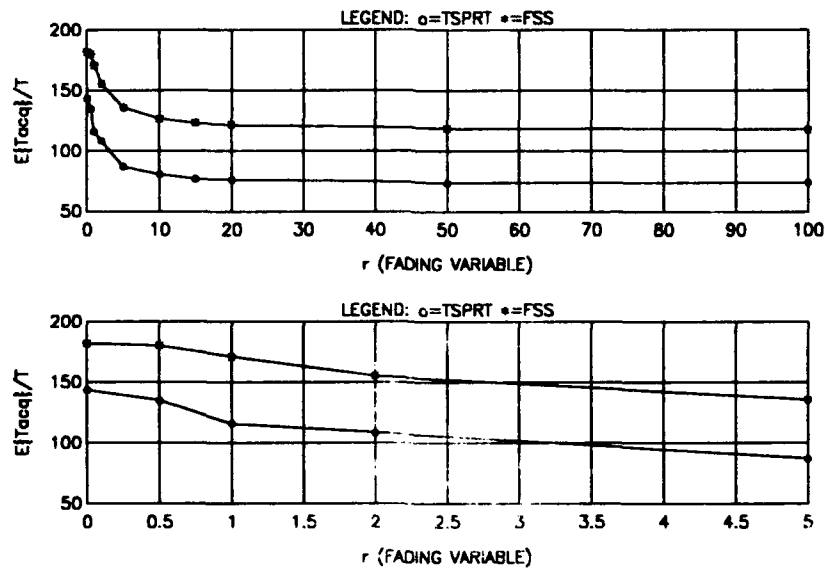

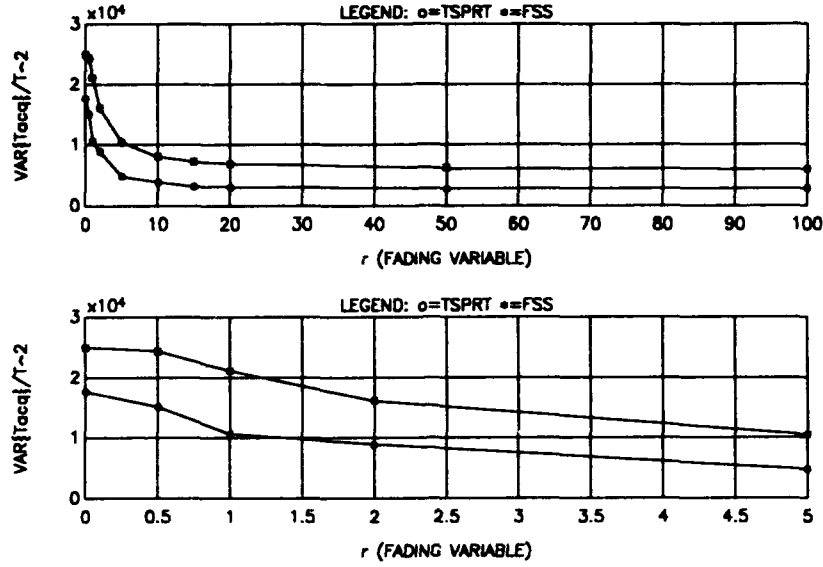Figure 4.1 The variation of μ_{TACQ} under fading conditions.

66

Figure 4.2 The variation of σ^2_{TACQ} under fading conditions.

2. Fading as a "Channel Mismatch" Problem

We have examined the channel mismatch problem for both of the FSS and TSPRT acquisition schemes in the previous chapter. We have shown that incoming signals that have different strength than predicted by the system designer caused performance degradation. Signals coming through fading multipath channel can be regarded as a specific case of channel mismatch.

Considering equation (4.9), one can see that under fading conditions, the reductions to the effective SNR would be due to a decrease in the mean of Gaussian quadrature components of the resulting Chi-squared test statistics (y_n) and an increase to the noise. The parameter λ_n is decreased by a factor of $[r / (1 + r)]$ and σ_n^2 is

increased by a factor of $(1 + [(\lambda_n/2\sigma_n^2) / (1 + r)])$. Since all our formulations are based on the ratio (λ_n/σ_n^2), we prefer to work on the equivalent normalized test statistics z_n (see (4.12)). With the help of equation (4.14), we can see that fading changes the parameters of z_n as

$$
\lambda_z = \begin{cases} \dfrac{\lambda_{n,1}}{\sigma_n^2} \rightarrow \dfrac{\lambda_{n,1}}{\sigma_n^2}\,\dfrac{r}{1+r} & \textit{under } H_1 \\[3mm] \dfrac{\lambda_{n,0}}{\sigma_n^2} \rightarrow \dfrac{\lambda_{n,0}}{\sigma_n^2}\,\dfrac{r}{1+r} & \textit{under } H_0 \end{cases}
$$

$$
\sigma_z^2 = \begin{cases} 1 \rightarrow 1 + \dfrac{(\lambda_{n,1}/\sigma_n^2)}{1+r} & \textit{under } H_1 \\[3mm] 1 \rightarrow 1 + \dfrac{(\lambda_{n,0}/\sigma_n^2)}{1+r} & \textit{under } H_0 \end{cases}
$$

(4.16)

Note that, since $\lambda_{n,1} > \lambda_{n,0}$ fading will effect our decision scheme differently under each of the two hypotheses.

Consider first the case under H_0. Since it represents a non-synchronization condition, ideally, i.e., complete random sequences were used, we should only detect noise after the correlation process in the receiver. However, since we are using a partial correlation receiver and an m-sequence, we treat the resulting small correlation value as if it were a "signal" under H_0. Our design assumes that $\lambda_{z,0} = (\lambda_{n,0}/\sigma_n^2)$ is upper bounded by per-chip SNR (see equation (2.13)), which is in this case 0.1, and fading further reduces this value. Therefore, we expect actually a slight improvement on the performance, but the slight increase in the noise variance counter effect the performance.

68

Therefore, we can conclude that fading has no or little effect on the performance of the acquisition scheme under H_0. This conclusion will later be confirmed by numerical results.

Under H_1, we see a completely different picture. In this case, we actually need a signal to detect the acquisition condition, and the higher this signal value is the better the performance. Unfortunately, fading affects this value adversely; it is decreased by a factor of $(r / (1+r))$. In addition to that, the noise variance (4.16) is increased in much greater pace than under H_0 (because $\lambda_{n,1} > \lambda_{n,0}$).

Our design approximates the parameter $\lambda_{z,1}$ ($= (\lambda_{n,1}/\sigma_n^2)$) as $nSNR(1-|\gamma|\Delta)^2$ (see equation (2.13)). Considering $SNR(1-|\gamma|\Delta)^2$ as a constant, $(\lambda_{n,1}/\sigma_n^2)$ is proportional to the sample size value n. Therefore the noise variance (4.16) is also increased with increasing n for a fixed r. We expect that the effects of fading to be severe for H_1 under these conditions.

The noncentrality parameter of the resulting test statistics is effectively decreased and underlying noise variance is increased due to the fading under H_1. Since the incoming signal plus noise appears to have less signal component and more noise component than no fading condition, the output of the correlator in the receiver tends to be more "H_0 like". Therefore, we expect a decrease in the effective probability of detection.

Considering equation (4.16), one can see that the worse the fading is the less the signal component and the more the noise, so that under the worst case (Rayleigh) fading the we will have no signal component but a noise which the variance at its

69

maximum. Since the noise variance also increases with increasing sample size for a fixed r, the output of the correlator tends more and more to be in the extreme regions (either H_0 or H_1) rather than in between, as the test length increases. The average sample size (ASN) is therefore expected to be decreased for worse fading conditions, i.e., the TSPRT will reach a decision earlier (not necessarily a correct one) because of the increased variance of the noise due to fading conditions.

We now present the numerical results for TSPRT to validify our discussion. Figures 4.3 and 4.4 depicts the variation of the aforementioned parameters under H_1 and H_0 for $\alpha=0.05$ and $\beta = 0.6, 0.8, 0.9$ and 0.99. We can see that the parameters under H_0, namely P_{fa} and $ASN_{2.0}$ essentially remain unchanged under fading, while $ASN_{0.5}$ and more importantly P_d behaves in the way we expected. The main cause of the performance degradation under fading is the degradation in the effective probability of detection. The decrease in the $ASN_{0.5}$ does not help, because the states under H_1 is just a small fraction of the total states (4 out of 2046 in our case), therefore, the reduction contributes very little to the overall average sample size per state and the resulting mean and the variance of the acquisition time.

Since the channel mismatch mainly occurs for H_1 and decreases the actual probability of detection, one corrective approach to reduce the effects of fading could be taken by increasing design β, while keeping α the same. Since the actual P_d will also increase, the system, therefore could satisfy a reasonable detection rate and perform better at severe fading conditions. But the increase in β will also result in an increase in the average sample size per state, therefore, the performance under no or less severe

70

fading conditions have to be sacrificed. To illustrate this, we raised the β value of our design example from 0.6 to 0.8,0.9 and 0.99. We rerun our simulation under the fading conditions represented by $r \in \{0\ 1\ 5\ 10\ 20\}$, for these values of β, while keeping all the other parameters constant. We present the results for μ_{TACQ} and σ^2_{TACQ} in Figures (4.5) and (4.6) respectively.
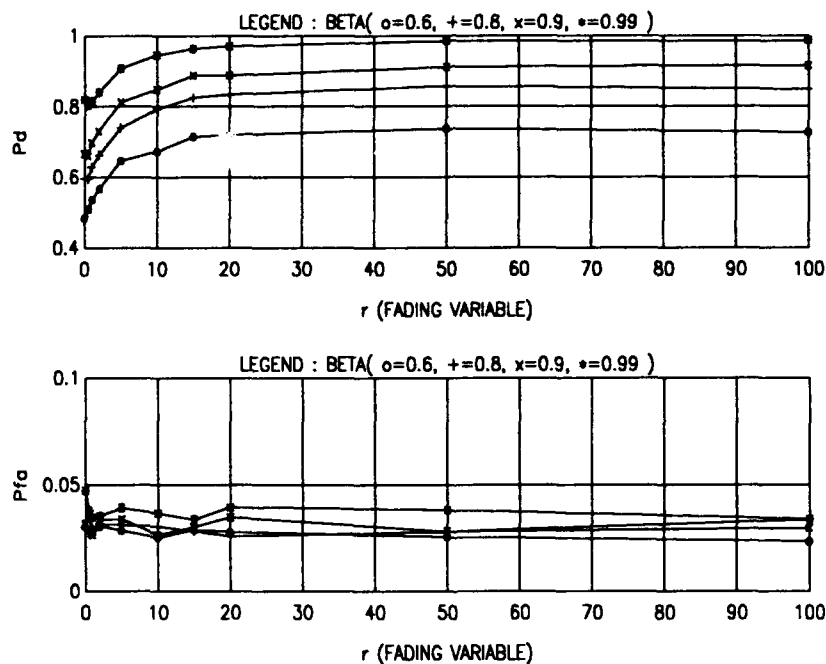

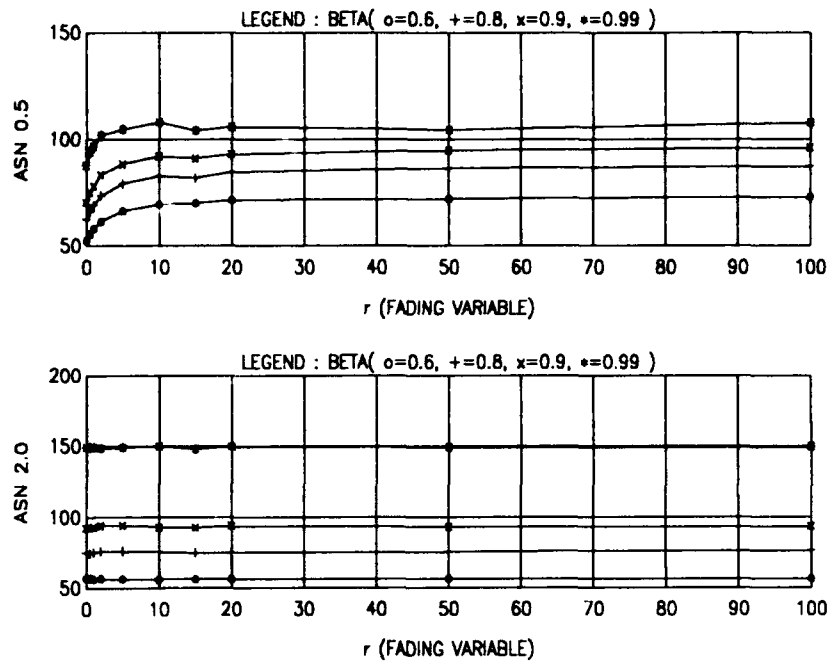Figure 4.3 The variation of actual P_d and actual P_{fa} for TSPRT scheme under fading.

71

Figure 4.4 The variation of $ASN_{0.5}$ and $ASN_{2.0}$ for TSPRT scheme under fading.
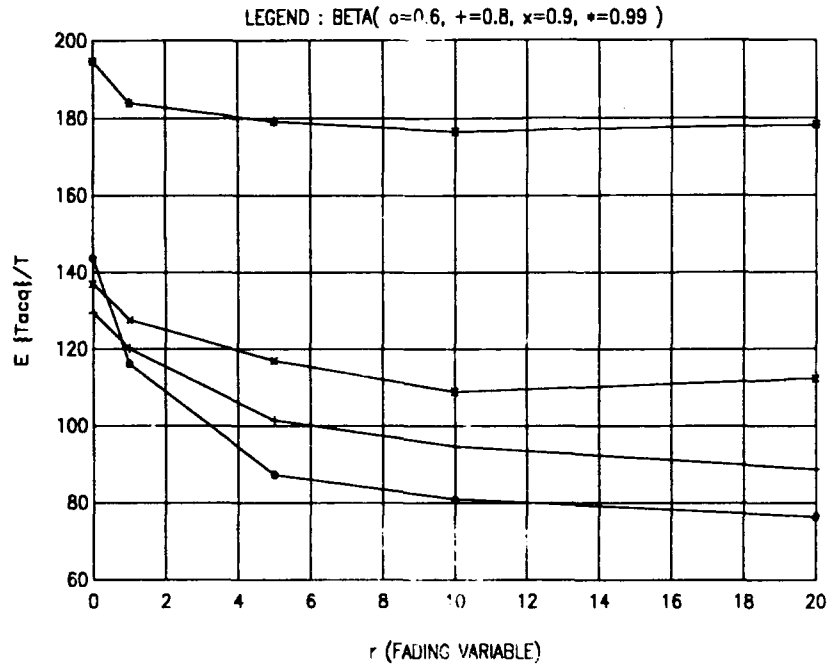

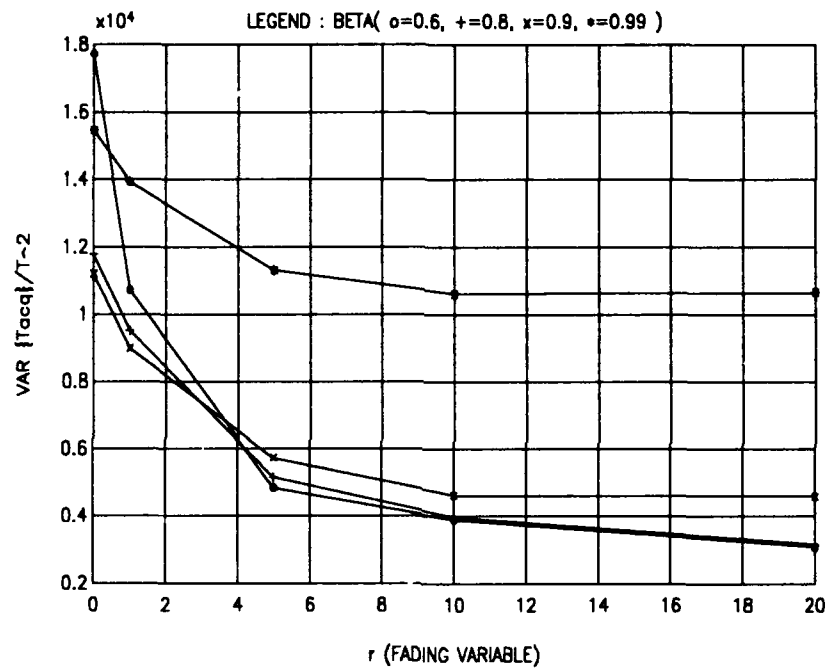**Figure 4.5** The variation of μ_{TACQ} under fading with various β.

Figure 4.6 The variation of σ^2_{TACQ} under fading with various β.

V. CONCLUSIONS

In this thesis, we have studied noncoherent PN code acquisition systems in terms of the mean and variance of the acquisition time in the classical AWGN channel and in the presence of slowly varying Ricean fading. We considered a single dwell fixed sample size (FSS) test decision scheme and a truncated sequential probability ratio test (TSPRT) decision scheme. The mean (μ_{TACQ}) and the variance (σ^2_{TACQ}) of the acquisition time was calculated using the flow-graph technique. We also assumed a majority logic verification scheme (coincidence detector) with early termination feature to reduce the effect of costly false alarms.

The design of either FSS or TSPRT scheme was based on specifying the desired false alarm probability and the desired detection probability, denoted by α and β, respectively. We have seen that there is an optimum set of (α, β) combinations which minimizes either μ_{TACQ} or σ^2_{TACQ} in the interval $[0,1] \times [0,1]$. The optimum value of α, denoted by α^* turned out to be very small, because the false alarms were costly and majority of the uncertainty phases fell into the category of non-acquisition conditions. On the other hand, the optimal β, denoted by β^* took moderate values (i.e., between 0.6 ~ 0.8). Our results suggested that it was not correct to assume that the mean or the variance of the acquisition time would be minimized with $(1 - \beta) \ll 1.0$, so that the correct phase cell was detected in the first sweep of the uncertainty region. Selecting a moderate β would result a much lower sample size per test than a high β, and this would

74

result in reduced μ_{TACQ} or σ^2_{TACQ} even though several sweeps of the uncertainty region might be required. The TSPRT scheme has been shown to perform much better than the FSS scheme in terms of these performance parameters. Approximate improvement of 57 % in the σ^2_{TACQ} and 38.3 % in the μ_{TACQ} were achieved by the TSPRT over the FSS scheme.

The effects of various penalty times to our design considerations were examined for the FSS scheme. We have seen that small variations in the penalty time did not interfere much in the selection of design parameters, but an excessive increase in the penalty time required a much lower α, whereas β remained essentially the same. We also saw that in case of uncertain penalty time, it was better to use the worst case value in the design.

We have examined the coincidence detector parameters and the early termination feature of the coincidence detector. We saw that it paid to employ a coincidence detection scheme in the system, for it greatly reduced the mean and the variance of the acquisition time. For the optimal selection of the parameters A and B, we found no simple solution, because these parameters depended on various system values. Our numerical results on the best cases suggested that A did not have to be so large, i.e., ≤ 5, and once A was fixed, optimum B turned out to be around $\lfloor A/2 \rfloor$, depending on the other system parameters. The early termination feature saved substantial time, especially if a large B value (close to A) was selected. The improvement was greatly reduced for smaller B values.

We have examined the operating point characteristics of the systems around the design per-chip SNR, what we called the *channel mismatch* problem. Our results showed that the performance degradation caused by weaker signals was far greater than the degradation caused by stronger signals and this degradation was more severe for higher design SNR values. Following this observation, we have concluded that if some uncertainty existed over the effective channel SNR, it was safer to design the system using the lowest possible SNR value to counterbalance the channel mismatch problem.

Finally, we have considered a slowly varying Ricean fading channel for both of the schemes. The TSPRT again performed better than the FSS scheme under fading conditions. We have seen that fading effectively reduced the actual detection probability under the hypothesis H_1 while the parameters under the hypothesis H_0 remained essentially unaffected. We have also seen that we could improve the performance under severe fading conditions by using a larger design β.

LIST OF REFERENCES

1. Schilling, D.L., and others, "Spread Spectrum For Commercial Communications," *IEEE Communications Magazine*, pp.66-78, April 1991.

2. Scholtz, R.A. "The Origins of Spread-Spectrum Communications," *IEEE Trans. Comm.* vol. COM - 30, pp. 822-854, May 1982.

3. Dixon, R. C., *Spread Spectrum Systems*, 2nd ed, John Wiley and Sons, 1984.

4. Cooper G.R. and McGillem C.D., *Modern Communications and Spread Spectrum*, McGraw-Hill, 1986.

5. Simon M.K., Omura J.K., Scholtz R.A., and Levitt B.K., *Spread-spectrum Communications*, Vol III, Computer Science Press, 1985.

6. Lehmann, E.L., *Testing Statistical Hypotheses*, Wiley, 1959.

7. Tantarantana, S., and Lam, A. W., "Noncoherent Sequential Acquisition of PN Sequences for DS/SS Communications," Proceedings 29th Allerton Conference on Communications, Control and Computing, Urbana-Champaign, pp. 370-379, October 1991.

8. Lam, A.W. and Tantarantana S., "Mean Acquisition Time for Noncoherent PN Sequence Sequential Acquisition Schemes," to appear in the Proceedings *IEEE* MILCOM 93, Boston, MA, October 1993.

9. Polydoros, A. and Weber, C. L., "A Unified Approach to Serial Search Spread-spectrum Code Acquisition - Part I: General Theory" *IEEE Trans. Commun.*, Vol COM-32,pp.542-549 , May 1984.

10. Vincent, P.J., "Effects of Fading and Data Modulation on Noncoherent M-sequence Acquisition Schemes", MSEE Thesis, Naval Postgraduate School, Monterey, CA, March 1992.

11. Helstrom,C.W. *Statistical Theory of Signal Detection,* Pergamon Press, 1968.

12. Brennan, L.E., and Reed, I.S., " A Recursive Method of Computing the Q Function," *IEEE Transactions on Information Theory,* VOL. IT-11, pp. 312-313, April 1965.

13. Papoulis, A, *Probability, Random Variables, and Stochastic Processes,* McGraw-Hill,1984.

14. Wald, A., *Sequential Analysis,* John Wiley and Sons, 1947.

15. Proakis,J.G., *Digital Communications,* 2nd ed, McGraw Hill, 1989.

INITIAL DISTRIBUTION LIST

		No. Copies
1.	Defense Technical Information Center Cameron Station Alexandria VA 22304-6145	2
2.	Library, Code 52 Naval Postgraduate School Monterey CA 93943-5002	2
3.	Professor Alex W. Lam, Code EC/La Department of Electrical and Computer Engineering Naval Post Graduate School Monterey, CA 93943-5000	4
4.	Professor Herschel H. Loomis, Code EC/Lm Department of Electrical and Computer Engineering Naval Post Graduate School Monterey, CA 93943-5000	1
5.	Deniz Kuvvetleri Komutanligi Personel Daire Baskanligi Bakanliklar, Ankara, Turkey	1
6.	Deniz Harp Okulu Komutanligi Tuzla, Istanbul, Turkey	2
7.	Golcuk Tersanesi Komutanligi Golcuk, Kocaeli, Turkey	1
8.	Taskizak Tersanesi Komutanligi Haskoy, Istanbul, Turkey	1
9.	Levent Misirlioglu Kaymakam Erkin Sokak 31/7 Yalova, Istanbul, Turkey	1